DOCTORAL THESIS

Adaptive Nonlinear Control for Energy-efficient and High-precision Motion of Industrial Feed Drive Systems

（産業機械送り駆動系の精密動作と省エネルギー化のための適応非線形制御）

Author:

Mathew Renny Msukwa

Supervisor:

Naoki Uchiyama

A thesis submitted in fulfillment of the requirements

for the degree of Doctor of Philosophy (Engineering)

in the

Systems Engineering Laboratory

Department of Mechanical Engineering

Toyohashi University of Technology

Toyohashi, Aichi, Japan

July, 2020

Declaration of Authorship

I, Mathew Renny Msukwa, declare that this thesis titled, "Adaptive Nonlinear Control for Energy-efficient and High-precision Motion of Industrial Feed Drive System" and the work presented in it are my own. I confirm that:

- This work was done wholly or mainly while in candidature for a research degree at this University.
- Where any part of this thesis has previously been submitted for a degree or any other qualification at this University or any other institution, this has been clearly stated.
- Where I have consulted the published work of others, this is always clearly attributed.
- Where I have quoted from the work of others, the source is always given. With the exception of such quotations, this thesis is entirely my own work.
- I have acknowledged all main sources of help.
- Where the thesis is based on work done by myself jointly with others, I have made clear exactly what was done by others and what I have contributed myself.

Signed: Mathew Renny Msukwa

Date: July, 2020

Abstract

Industrial feed drive systems, particularly ball and lead-screw feed drives, are among the most dominating motion components in the production and manufacturing industries because of their wide range of applications, such as in multi-axis motions. The growing demand for precise products poses the need for high-speed production systems with higher accuracy. In addition, feed drive systems operate around the clock all over the world; hence, they are among the major consumers of the industrial energy supply. While high-speed motion is preferred, it causes mechanical vibration in light systems, insufficient accuracy, and high-energy consumption. The control performance greatly depends on the systems' vibration, unmodeled uncertainties, and external disturbances. In machining, two main control approaches are used to enhance precision: tracking control approach and contouring control approach. The contour error is defined as the component orthogonal to the desired contour curve, which represents a better indicator of precision machining. However, calculating the contour error in real time is difficult because it requires solving a nonlinear equation in real time. This dissertation discusses several approaches to improve precision of industrial feed drive systems,

1. We present an adaptive sliding mode controller (ASMC) with a nonlinear sliding surface for ball-screw feed drive systems to enhance the tracking performance and reduce the consumed energy of industrial feed drive systems. Employing an ASMC results in an enhanced tracking performance and less energy consumption compared to nonadaptive sliding mode control. The energy consumption is reduced by 13.3 %, while the control input variance is reduced by 15.2 %.

2. We extend the proposed ASMC and consider adding a feed forward compensator to improve the machining accuracy and reduce the consumed energy of industrial feed drive systems. The advantage of including the uncertainty compensator is that it cancels out the effect of uncertainties that may exist in a plant, thereby improving the performance. Compared to the ASMC, the proposed approach achieves a substantial tracking performance, wherein the average tracking error is reduced by 33.3 %, and the energy consumption is reduced by 2 % under a similar tracking performance.

3. The most significant factor in machining is the accuracy of the overall system or the system's contour error. Therefore, we propose herein a combined approach of the adaptive sliding mode contouring controller (ASMCC) with reference adjustment and the sliding mode controller based on uncertainty dynamics. The controller aims to enhance the contouring performance by explicitly considering reference adjustment with the addition of the uncertainty dynamics compensator. The proposed approach shows a substantial improvement in performance by reducing the average contour error by 85.71 % and the maximum contouring error by 78.64 %.

Acknowledgements

First, I would like to thank God Almighty Father for giving me good health, strength, knowledge, ability, and opportunity to undertake my doctoral studies, hold on, and complete it satisfactorily. Without His blessing, this would not be possible.

I place in record my sincere gratitude to my advisor Prof. Dr. Naoki Uchiyama. I am extremely grateful and indebted to him for his expert, sincere and valuable guidance and encouragement, which he has extended to me all throughout the course of my studies, and his willingness to continue guiding me on further studies.

I also take this opportunity to express my sincere gratitude to my committee members: Prof. Dr. Kaiji Sato and Prof. Dr. Naohiro Fukumura for their support and constructive comments. Furthermore, I would like to express my sincere thanks to all the members of the Systems Engineering Laboratory for their feedback, cooperation, and friendship.

A very special gratitude goes to Toyohashi University of Technology for helping me and providing the funding for my studies.

Last, but not the least, I would like to thank my family - my parents and relatives for always supporting me unconditionally. I am forever grateful. Special thanks to my brother, Dr. Kenneth Renny Simba, and his family who have been here in Japan with me since I came. They have always supported me academically and in life in general.

Mathew Renny Msukwa

Contents

List of Figures

List of Tables

Chapter 1

Introduction

1.1 Introduction

The demand for high performance placed on machine tools from end users, such as the aerospace, automotive, die, and mold industries has greatly increased over the years. The aerospace industry requires high-speed machine tools that enable complex parts to be produced in one piece within the shortest possible time. Meanwhile, the die and mold industries require machine tools that can cut complex three-dimensional shapes with speed, accuracy, and high-quality surface finishes. Likewise, automotive manufacturers need high-precision machines that can perform point-to-point cutting operations in minimum time [1]. In response to these demands of high speed and precision, computer numerical control (CNC) machines have been an indispensable key.

1.1.1 Computer Numerical Control Machines

In a CNC machine, a computer and a program are used to control, automate, and monitor the movement of a machine tool. The machine can be a milling machine, lathe, router, welder, grinder, laser or waterjet cutter, sheet metal stamping machine, robot, or many other machine types. This program contains coded alphanumeric data, which are used

to control workpiece or tool motions. In addition, the program includes some input parameters (e.g., feed, cut depth, and spindle-speed) and functions (e.g., turning spindle on/off and turning coolant on/off).

Accordingly, CNC machines have many advantages over conventional manufacturing machines. These advantages include high manufacturing accuracy, short production time, greater manufacturing flexibility, contour machining (two to five-axes machining), and reduced human error, among many others. CNC machines are widely used in the machine tool area because of these advantages. However, CNC has some drawbacks, such as high cost, maintenance, and skilled part programmers.

1.1.2 Feed Drive System

CNC machines generally consist of a group of axes known as feed drives. Each axis has a driving motor that provides the driving forces for linear axes or torques for rotary axes. This force or torque is transmitted to the axis through a train of mechanical transmission elements such as gears. Ball-screw feed drives have the advantages of low cost, robustness to disturbances, high stiffness against cutting forces, high gear ratio, and high table load variations. Therefore, ball-screw drives are frequently used in machine tools. Fig. 1.1 shows a typical structure of ball-screw feed drive systems [2]. The driving system provides the torque and linear motion of the feed drive through the ball-screw mechanism. A servo motor is attached at one end, and it provides the torque required by the system. The torque is transmitted to the ball-screw shaft through a transmission mechanism, (e.g., coupling or gears). The ball-screw changes the rotational motion of the motor into a linear motion of the table holding the work piece or the spindle holding a cutting tool.

Another method of providing the linear motion of the feed drive is to employ direct drives, such as linear motors (Fig. 1.2), in which the linear motion and the thrust are directly supplied to the machine tool table without needing an intermediary conversion mechanism.

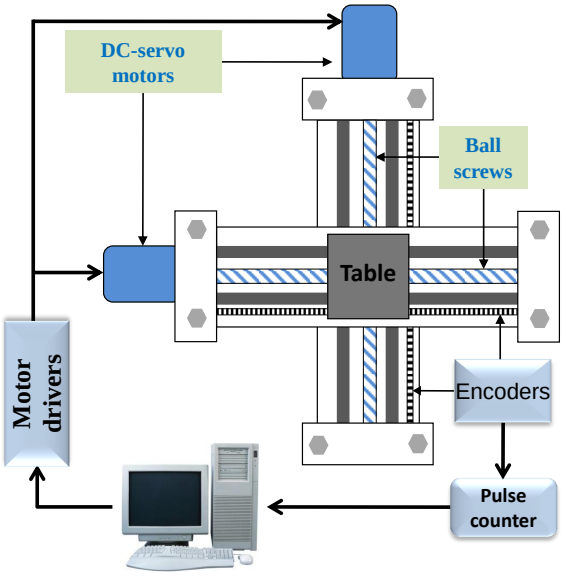

FIGURE 1.1: Feed drive system structure

In other words, direct drives have an advantage over ball-screw drives because they involve fewer components and are less susceptible to the influence of undesirable structural modes [1]. Another advantage of linear actuators is that they can achieve higher speeds and accelerations with minimal backlash and friction. On the contrary, direct drives suffer from some significant drawbacks, such as high sensitivity to changes in workpiece mass. Their dynamic stiffness mainly depends on the controller settings. In addition, it has little reinforcement from the mechanical structure. As a result, the large forces that occur during machining could easily excite the dynamics of the control loop and cause instability in both the controller and the metal cutting process. To mitigate the effects of the cutting forces and workpiece mass variations on the control of direct-driven machines, they are typically oversized by increasing the table mass and the linear motor power.. This consequently reduces the achievable bandwidth and increases the cost of direct-driven machine tools, which are both undesirable [1].

In machining applications, the interpolator generates the desired tool motion relative to the workpiece and then decomposes the desired motion into reference position commands

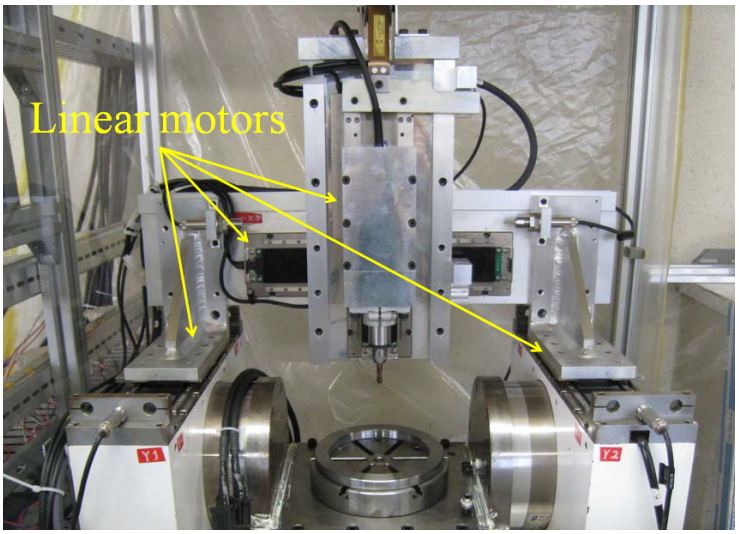

FIGURE 1.2: Application of linear motor in CNC machines

for individual driving axes. High-precision position control full-closed feedback control is applied to achieve high speed. Accordingly, several control approaches have been proposed for such a system. Proportional position control and proportional plus integral velocity control or integral plus proportional velocity control (P, PI/I-P), which is a type of proportional plus integral plus differential control, are generally applied in many industrial applications. However, when changing the mechanical characteristics of the control target, the P, PI/I-PI control parameters must also change to maintain a good motion performance [3].

1.1.3 Control of Multi-axis Feed Drive Systems

In industrial machines, ball-screw feed drives are frequently used to position the spindle or table to the desired location because of their high stiffness and accuracy. The positioning precision and efficiency directly determine the quality and the productivity of machine tools [4]. Hence, one must possess insight of control methods to achieve a high accuracy. Some challenges are associated with controlling any type of feed drive system (i.e., whether

it is ball-screw-driven or direct drive-based). Achieving a high positioning accuracy at elevated speeds and accelerations, maintaining a sufficient amount of stiffness over a wide frequency range for disturbance force rejection, and delivering a specified performance in a robust manner are difficult in the presence of acceptable variations in the feed drive's dynamics. With the recent advances in high-speed machining, maintaining the dynamic tool positioning accuracy has become more important than ever before to be able to take advantage of the productivity gains facilitated by high cutting speeds [5].
Different control approaches have been studied in the literature to enhance the performance of feed drive systems. This section addresses a brief review on the basic control of feed drive systems.

Feedback Controllers

Simple controllers like the proportional derivative, proportional integral, and proportional integral derivative (PID) controllers are the most commonly used control loop feedback controllers in industrial control systems. The PID controller continuously calculates an error value as the difference between a desired/reference setpoint and a measured process variable and applies a correction based on the proportional, integral, and derivative terms. In a PID controller, the control signal is the summation of the proportional, integral, and derivative components of the position error. Fig 1.3 shows a typical PID feedback controller for a single-axis feed drive system. The control loop is turned by adjusting the proportional (K_p), integral (K_i), and derivative (K_d) gains to the optimum values for the desired control response. Aside from their simplicity, which reduces engineering effort, the other advantage of PID controllers is their requirement of minimum knowledge on the process to be controlled. The major weakness of PID controllers is that poor feedback tuning may cause instability and yield a poor tracking performance at corners.

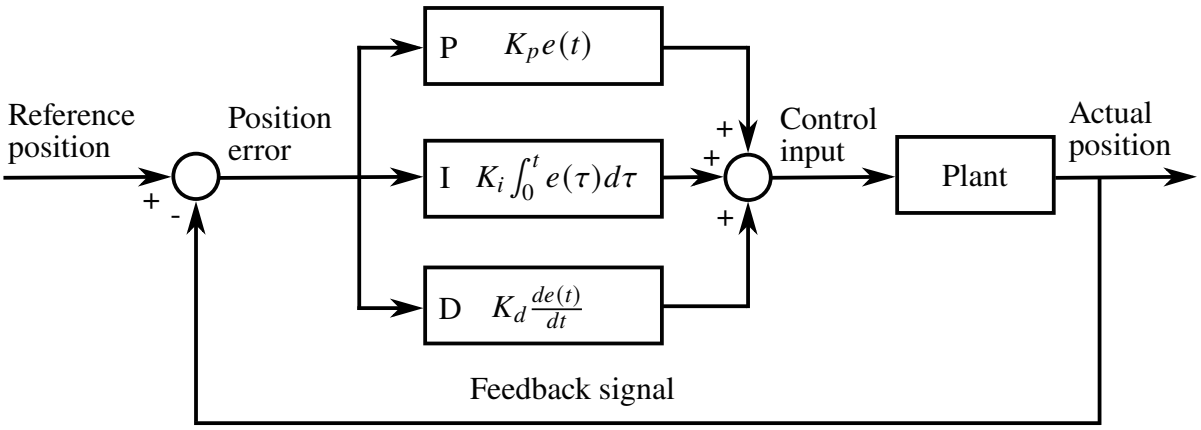

FIGURE 1.3: Feedback controller for single axis feed drive system

Feedforward Controllers

Consider the poor tracking performance of feedback controllers, a feedforward controller is added to the control loop to predict the desired control signal and improve the tracking accuracy. Feedforward controllers use prior knowledge on the reference trajectory to predict an approximate control signal and incorporate it with the feedback controller to achieve accurate tracking. Feedforward controllers aim to predict an approximate control signal and use it to cancel the almost dominant control force, thereby enabling the feedback controller to focus on compensating for minor disturbances. Tomizuka [6] proposed the Zero Phase Error Tracking Controller (ZPETC) that achieves a wide bandwidth with zero phase delay. However, the control method with the ZPETC requires a very accurate identification of the feed drives' transfer functions, which should be time-invariant. The tracking performance of the ZPETC or other feed-forward controller is highly degraded with the variation of the feed drive parameters [7].

Robust Controllers

Robust controllers focus on making control systems robust against uncertainties in the drive parameters, maximizing the bandwidth within the physical limitations of the system,

and compensating for external disturbances. However, these controllers still focus on improving the individual axis performance only. The main drawback of these methods, which consider the performance of each axis separately during contouring, is that reducing the individual axis errors does not necessarily reduce the contour error. The sliding mode [8, 9] and H_∞ controllers [10] are examples of robust controllers.

Cross-coupling Controllers

Cross-coupling controllers are widely applied to eliminate the contour errors in contour-following applications instead of reducing individual axis errors. Therefore, a cross-coupling controller requires the construction of a contour error model in real time and its utilization in a control law that reduces the contour error. Ref. [11] proposed a cross-coupled controller (CCC) by calculating the contour error from the tracking error in biaxial contour-following tasks. The authors in Ref. [12] employed a cross-coupled fuzzy-logic controller for improving the contouring accuracy. In their design, they utilized a new fuzzy rule-generated method based on the performance index of the contour error model. Fig. 1.4 depicts the block diagram of a basic biaxial cross-coupling controller. The axial position errors e_x and e_y were used to calculate the contour errors ε by multiplication by the variable gains, C_x and C_y. The output of the proper control law is decomposed into two axial components by multiplication by C_x and C_y. These axial components were then inserted into individual axis loops with the appropriate sign ensuring that contour error correction was executed in the proper direction. However, the minimization of the tracking error in the CCC achieved by the axial controller does not reduce the contour error, thereby forcing the contour controller to contradict it. Consequently, judging which controller dominates the contour error has become difficult, hence, some difficulties in adjusting the controller parameters will appear.

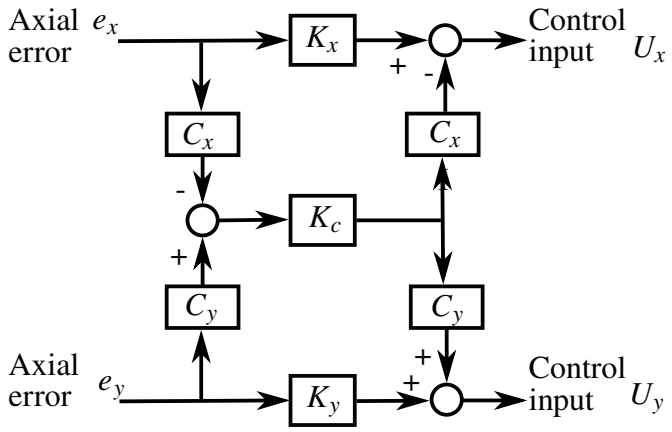

FIGURE 1.4: Cross-coupling controller for a biaxial feed drive system

Contouring Controllers

Contouring control is a controller design that considers the error components orthogonal to the desired contour curves, called "contour error" as feedback signals. Reduction the error components orthogonal to the desired curves is effective in contour following in multi-axis machining tasks. Ho *et al*. decomposed the contour error into a normal tracking error and an advancing tangential error, following which a dynamic decoupling procedure was applied to the system dynamics [13]. The authors in Ref. [14] proposed the task coordinate frame approach by transforming the machine tool feed drive dynamics into a moving-task coordinate frame attached to the desired contour. Meanwhile, the authors in Ref. [15] proposed an integrated control scheme comprising a feedback controller, a feedforward controller, and a modified contour error controller (i.e., a CCC equipped with a real-time contour error estimator). In addition, they also proposed a fuzzy -logic-based feed rate regulator to further reduce the contour error. Su and Cheng [16] proposed a position error compensator (PEC) by compensating for the position errors in advance. They further reduced the contour error by employing an integrated motion control scheme consisting of a PEC, a modified version of the CCC, and a fuzzy -logic-based feed rate regulator. Lo and Chung proposed a tangential-contouring controller for the biaxial

motion [17]. The proposed controller was based on a coordinate transformation between the *XY* and tangential contouring (T C) frames defined along the contour. Cheng and Lee proposed a real-time contour error estimation algorithm [18]. Ye *et al*. proposed a new cross-coupled path pre-compensation algorithm for rapid prototyping and manufacturing systems [19]. Meanwhile, Tarng et al. presented a cross-coupled fuzzy-feed rate control scheme to reduce the contour error by optimizing the controller parameters using a genetic algorithm [20]. Chin *et al*. proposed a fuzzy-logic controller to a proven algorithm in the cross-coupled pre-compensation method and used both position and contour error to generate the compensation term [21]. Yeh and Hsu [22] proposed an adaptive feed rate interpolation algorithm based on the geometric relationship between the chord error and curvature constraints. Jee and Koren proposed an adaptive fuzzy logic controller to reduce the contour error [23]. They simultaneously adjusted both input and output membership functions within a stable range derived from a stability analysis.

Adaptive Controllers

Adaptive control is a type of control method used by a controller, which adapts to a controlled system with varying parameters or is initially uncertain. Adaptive control is different from robust control in that it does not need a priori information about the bounds on these uncertain or time-varying parameters. Robust control guarantees that if the changes are within the given bounds, the control law need not be changed. Meanwhile, adaptive control is concerned with the control law changing itself.

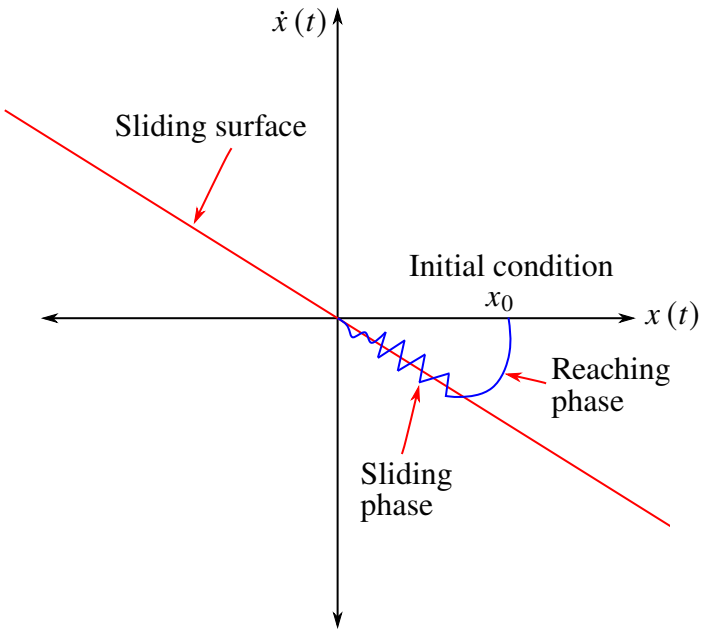

FIGURE 1.5: State trajectory during reaching phase and sliding phase in sliding mode control.

1.2 Sliding Mode Control

1.2.1 Introduction

In control systems, sliding mode control (SMC) is a particular type of variable structure control system that alters the dynamics of a nonlinear system by applying a discontinuous control signal that forces the system to slide along a cross-section of the system's normal behavior. The state-feedback control law is not a continuous function of time; instead, it can switch from one continuous structure to another based on the current position in the state space. SMC originated in the Soviet Union sometime in the late 1950s, but it was not published outside the Soviet Union until the works of Refs. [24] and [25] were published. After these publications, the list of publications concerning SMC grew rapidly, and SMC has been receiving increasing attention in many control fields, such as electromechanical systems, robotic manipulators, and servo systems.

SMC has many attractive features. Some of its features are its relatively simple design, invariance to systems dynamic characteristics and external disturbances, control of independent motion as long as sliding conditions are maintained, and wide variety of operational modes, such as regulation, trajectory control [26], mode following [27], and observation [28]. However, SMC has already been studied in many reports [29–32], surveys [33], and books [24, 34, 35] and remains the object of many studies from the theoretical viewpoint or related to various applications [36].

The following first-order uncertain system is considered [37] to understand the sliding mode control approach.

$$\dot{x}(t) = ax(t) + bu(t) + \rho(x,t), \tag{1.1}$$

where $x(t) \in R$ and $u(t) \in R$ are the control variable and control input, respectively. a and b are known nonzero constants. $\rho(x,t) \in R$ refers to the unknown uncertainty, and only the bound of this uncertainty is known. To stabilize the system in 1.1, if the initial value of $x(t)$ is positive, then $x_(t)$ should be negative, and vice versa. Therefore, depending on the sign of $x(t)$, the control law should be altered to ensure $x(t)$ stabilization. Let us consider the following control law:

$$u(t) = -b^{-1}(ax(t) + Q\text{sgn}(x)), \tag{1.2}$$

where, sgn(.) denotes the sign function, and $Q > 0$ is chosen such that

$$Q \geq \rho_{max}. \tag{1.3}$$

ρ_{max} represents the upper bound of the uncertainty $\rho(x,t)$. With the control law 1.2, system 1.1 becomes

$$\dot{x}(t) = -Q\text{sgn}(x(t)) + \rho(x,t). \tag{1.4}$$

Three different cases are considered to analyze the the above closed-loop system. The first involves the initial condition of $x(0) > 0$ 1.4 shows that $\dot{x}(t) < 0$. Therefore, $x(t)$ is decreasing and moving toward the origin $x(t) = 0$. The Second case involves the initial condition of $x(0) < 0$. Using 1.4, implies that $\dot{x} > 0$. Therefore, $x(t)$ is increasing and approaches $x(t) = 0$. The third case denotes that the discontinuous part of the control law is not defined when $x(t) = 0$. However, the moment the trajectory crosses the surface $x(t) = 0$ from either direction, it is again forced back on $x(t) = 0$ according to the abovementioned two cases. Therefore, $x(t)$ is moving toward the surface $x(t) = 0$ in all cases. The control law 1.4 forces the system state $x(t)$ to $x(t) = 0$, regardless of the initial conditions.

Fig. 1.5 shows the state trajectories in the vicinity of the sliding surface $s(x,t) = 0$. The sliding mode control has two phases Fig. 1.5. The initial phase when the trajectory is forced toward $x(t) = 0$ is called the reaching phase. The second phase when $x(t) = 0$ is called the sliding phase or sliding mode. The external disturbance can affect the system performance during the reaching phase. Meanwhile, the system motion is insensitive to the external disturbance during the sliding phase. The control law on $x(t) = 0$ is discontinuous and requires switching at a very high frequency to maintain the system on the desired sliding surface. If switching occurs at a very high frequency, then $x(t) = 0$ can consistently be maintained with this discontinuous control law.

1.2.2 Nonlinear Sliding Surface Design

The design of the sliding mode control generally consists of two main steps. The most crucial and important step in the sliding mode control design is the construction of the sliding surface expected to respond to the desired control specifications and performance [38]. The second step in the sliding mode control design procedure is the determination of a control law that forces the system dynamics to the sliding surface within a finite time and remains on it for a subsequent time. The sliding control law generally consists of two terms: the continuous control law that controls the system on the sliding surface and the discontinuous control law that guarantees stability against the disturbance effect. A linear sliding surface, which gives a constant damping ratio, is utilized in the conventional sliding mode controller design. In many control system applications (e.g., robotics, electric drives, machine tool control, and vehicle and motion control), the most important requirements are fast response and small overshoot. However, a quick response produces a high overshoot, which causes contour errors and increases the consumed energy. On the contrary, a low overshoot means a slow response, which leads to significant contour errors. Thus, achieving a small overshoot with a fast response using the conventional linear SMC method is very difficult. This particular problem can be solved by employing the composite nonlinear feedback technique [39]. The nonlinear sliding surface consists of linear and a nonlinear terms. The linear term comprises a gain matrix with a very low damping ratio value, thereby facilitating a fast response [40]. Meanwhile, the nonlinear term is introduced to provide a variable damping ratio to achieve small overshoot and settling time of the closed-loop system as the contour error converges to zero.

1.3 Manufacturing and Environment

Manufacturing is one of the major activities in industries that is responsible for a large portion of the total energy consumed in this sector, making it the key point in environmental impact studies [41]. Performing machining processes with better energy efficiency can significantly enhance the environmental performance of the manufacturing process and systems. Energy analyses have shown that the cutting energy used in the machine tool in the material removal process accounts for 15-25 % of the total energy consumed by the machine [42–44]. This energy consumption can be categorized as that consumed by the main spindle and the feed drives. Researchers recently developed several approaches in the process control level to reduce the energy consumption in machining by improving the tool chip contact mechanics. For example, Ref. [45] proposed diamond-like carbon-deposited tools to enhance the energy efficiency of machine tools. However, note the mean power consumed by feed drives during roughing operations is smaller than the power consumed by the spindle. In addition, they have non-negligible power consumption compared to the spindle during the finishing operations. The feed drive is also used for other operations, such as the returning motion of the tool. We focused herein on the feed drive motion. Most industrial robots, in which the energy consumed by the feed drives contributes a large proportion to the total power consumption, can apply this idea.

1.4 Thesis Outline

The remainder of this thesis is organized as follows: Chapter 2 presents the design and experimental verification of adaptive sliding mode control using a nonlinear sliding surface that reduces energy consumption while providing a satisfactory tracking performance; Chapter 3 describes an adaptive sliding mode controller design with a feedforward compensator for the energy-efficient and high-precision motion of feed drive systems; Chapter

4 introduces an extended version of the proposed design presented in Chapter 3 to adaptive sliding mode contouring control (ASMCC) for feed drive systems, which mainly aims to enhance the contouring performance by explicitly considering reference adjustment with the addition of the uncertainty dynamics compensator (note: the proposed method enhances both the tracking and contouring performances of feed drive systems while maintaining the required energy); and finally, Chapter 5 presents the conclusion and future work.

Chapter 2

Adaptive Sliding Mode Controller Design with a Nonlinear Sliding Surface for the Feed Drive Systems

2.1 Introduction

Energy sources must be used efficiently considering the limited reserve of nonrenewable energy sources and environmental factors, such as global warming and climate change [46], [47]. The industrial community, particularly the manufacturing sector, is estimated to deplete approximately $1/3$ of the world's energy consumption [48]. Reducing the energy consumption in industrial machines can reduce the overall production costs and enhance industrial competitiveness. Production machines, such as machine tools, operate continuously for a long time. Even a small percentage of energy reduction can effectively lower the production costs and reduce the environmental damages caused by energy generation systems. Feed drive systems generally take the highest percentage of motion systems in the industrial community and are widely applied in CNC machines, industrial robots, and precision assembly equipment, among others. These applications are considered as one of the major sources of high-energy consumption because they run for a long time all

over the world. Hence, the optimization of energy consumption in industrial machines is critical and increasingly attracting many researchers [49–57].

Although several methods for enhancing the motion of feed drive systems have been proposed in former studies, great efforts were required for developing controllers to improve the tracking performance of each industrial system [58–67]. Furthermore, responding to the demand for high-speed machining, recent studies concentrated on controllers that could improve the machining accuracy. Machine tools are normally composed of linear motion segments, that limit the machine movement for certain geometries and compromise the precision of machined parts. Several studies came up with interesting methods for generating smooth trajectories and developing controllers for high-speed motions [68–70]. To meet these requirements, a survey of the recent literature showed that SMC is recognized as a sufficient tool for designing robust controllers for complex high-order nonlinear dynamic plants operating under various uncertainty conditions [55, 70–74]. SMC has many good features including invariance to matched uncertainty, robustness against perturbation, and simplicity in design. Adaptive nonlinear sliding mode control with a nonlinear sliding surface for feed drive systems was designed in Ref. [75]. Its effectiveness was also verified.

Despite the previous studies, a comprehensive literature review in energy consumption modeling and energy efficiency evaluation for energy-saving in manufacturing is required because some related concepts are not clear, and the precision models still need to be promoted in this field [46]. While some studies, such as that of Ref. [47] focused on integrating the machine selection and operation sequence for reducing the energy consumption of the machine tools, the control design can be used as an inexpensive and effective approach toward energy saving while enhancing machining accuracy. Simultaneous efforts for enhancing the tracking performance and reducing the energy required to operate industrial machines, especially feed drive systems, are the key motivation for this

study.

In our previous studies, several methods for controlling the feed drive systems, including a novel sliding mode controller with a nonlinear sliding surface, were proposed to reduce the energy consumption in a ball-screw feed drive system [76]. With the nonlinear sliding surface, the damping ratio of the control system can be changed from a low initial value to a high final value to achieve a fast system response without an overshoot. Hence, a better performance with less energy consumption is simultaneously achieved. The effectiveness of using a nonlinear sliding surface in reducing the energy consumption by a feed drive system was proven. The energy consumption was reduced by approximately 12.9 % compared to the sliding mode control with a linear sliding surface. Despite the good performance of the controller proposed in [76], its design requires knowledge of the uncertainty bound that practically could be a difficult task to know. In case this bound is overestimated, it will yield excessive gain, which implies a higher control input magnitude that unnecessarily causes higher energy consumption.

For good performance of electromechanical systems, robust controllers like the sliding mode control (SMC) and the H_∞ has been considered by many researchers. These controllers guarantee that if changes occurring in system's parameters are within given bounds, the control law need not be changed. By making the robust controllers adaptive, there may be no need of prior information about the bounds of uncertain or time varying parameters. In our research we mainly focus on variable structure control, particularly adaptive sliding mode control (ASMC) because sliding mode controllers provide a viable and effective method with a strong robustness property and fast error convergence characteristics for nonlinear systems subjected to external disturbances and parameter variations by emulating a prescribed reduced-order system [77].

The following are some of the old (1989 to 2008) robust control studies. In Ref. [78], the authors has reviewed some of the main contributions on robustness of adaptive controllers

and some future research areas and problems have been identified. Some interesting open questions have been provided. Finaly, the authors concluded that the field was still in its early stages of development with lots of promising approaches but very little definite answers.

SMC for discrete time systems was proposed in Ref. [79]. The main feature of this approach is the reduction of the order of the relevant error equation, and the possibility of dealing with the nonmatched uncertainties introduced by the sampling process. However, the design only focus on reducing trajectory tracking errors, and no energy saving was considered.

A stable adaptive fuzzy sliding mode controller for nonlinear multi-variable systems with unavailable states was proposed in [80]. The proposed controller showed that uniformly asymptotic output feedback stabilization can be achieved with the tracking error approaching to zero. However, energy saving was not considered. Also no experiments were conducted to confirm the effectiveness of the proposed controller.

The authors in Ref. [81] proposed an adaptive sliding mode control with the sliding variable $\sigma(x,t)$ for nonlinear systems with uncertain parameters. An adaptive control gain $K(t)$ was given by $K(t) = \bar{K} \cdot |\eta| + \chi$ with $\bar{K} > 0$, $\chi > 0$, and η is the average of sign(σ) obtained through a low pass-filter $\tau \cdot \dot{\eta} + \eta = \text{sign}(\sigma(x,t))$ with $\tau > 0$. The main advantage of this controller is the adjustment of the control gain by using the equivalent control concept. This means that chattering is decreasing. However, the K-adaption law needs the knowledge of uncertainty bounds. Furthermore, the use of low-pass filter introduces in the closed-loop system dynamics with τ parameter that is not easy to tune and transient phenomena in case of uncertainties. Apart from that, the methodologies for tuning τ and χ have not been explained except their positivity and that the time constant of the low-pass filter τ must be small.

In [82], the authors proposed an adaptive sliding mode control with the sliding variable

$\sigma(x,t)$ for nonlinear systems with uncertain parameters. An adaptive control gain $K(t)$ was given by $\dot{K} = \bar{K} \cdot |\sigma(x,t)|$ with $\bar{K} > 0$ and $K(0) > 0$, then there exists a finite time $t_F \geq 0$ so that the sliding mode is established in system for all $t \geq t_F$, i.e $\sigma(x,t) = 0$ for $t \geq t_F$. One main feature of this approach is that prior knowledge of control gain is not required. However, from the $K-$dynamics, it yields that when $\sigma = 0$, $\dot{K} = 0$ (since $\dot{K} = \bar{K} \cdot |\sigma|$). In this case, the gain K is clearly overestimated with respect to uncertainties, which induces large chattering. Furthermore, this design is applicable only for ideal sliding mode, the objective $\sigma = 0$ being reachable. For the case of real sliding mode, $\sigma = 0$ is not reachable, causing the gain K gain to increase always. The authors proposed to modify K-dynamics by introducing boundary layer neighbouring the sliding surface $\sigma = 0$. This means that accuracy has to be sacrificed in order to apply the previous controller and that the control gain is still overestimated.

A control approach for speed tracking and synchronization of multiple motors by incorporating an adaptive sliding mode control technique into a ring coupling synchronization control structure was developed in [83]. An adaptive law is exploited to estimate the unknown bound of uncertainty, which is obtained in the sense of Lyapunov stability theorem to minimize the control effort and attenuate chattering. However, apart from extensive simulations, no experiments were conducted to verify the effectiveness of the proposed control scheme.

There are also several recent robust control studies, for example in [84–86]. In [84], an observer-based adaptive sliding mode control for nonlinear Markovian jump systems (MJSs) was designed. Firstly, an observer is constructed to estimate the system state. Then, an integral sliding mode surface and observer-based adaptive sliding mode controller such that the MJSs are insensitive to all admissible uncertainties and satisfy the reaching condition. However, in this design only a numerical example is exploited to demonstrate the effectiveness of the proposed results.

Meanwhile, a sliding mode contouring control with a nonlinear sliding surface and a gain scheduling technique for feed drive systems was proposed in [85]. Through a simulation analysis, the authors showed that this method could reduce the contour error by approximately 31.48 % without any change in the energy consumption compared to the nonadaptive sliding mode control. Although the controller was considered as an adaptive sliding mode control, the adaptive gain was chosen based on the adaptive law in [86] and modified to $K_c = \int \rho S_m^2 dt$, where ρ is the positive scalar adaption rate, and S_m is the sliding variable. In other words, the adaptive gain continues to increase until the upper limit is reached. The problem with this adaptive law is that K_c affects the control input only during the reaching phase. The adaptive law has no impact on the control input when the sliding variable is equal to zero (sliding phase). Furthermore, no analysis was provided as to how energy can be saved using this method. Both the reaching and sliding phases should be considered when designing adaptive sliding mode control to save energy in feed drive systems.

The design and experimental verification of the SMC using a nonlinear sliding surface for reducing the energy consumption were proposed herein based on the earlier discussion to raise awareness on the energy issues in feed drive systems and elaborate the advantages of the SMC in reducing energy consumption while providing a satisfactory performance. The stability of the proposed control system was proven using the Lyapunov stability theory, wherein the system trajectories converged to the sliding surface. Simulation and experiments were performed to confirm the effectiveness of the proposed method. Subsequently, the results were compared to those of the controller in Ref. [76], which was a nonlinear sliding mode control with no adaption. The proposed method achieved a better performance by reducing the energy consumption by 3.4 % and the tracking error by 46 % with a trifolium trajectory. In addition, the control input variance was reduced by 12.6 %. The remainder of this chapter is organized as follows: Section 2.2 presents the system

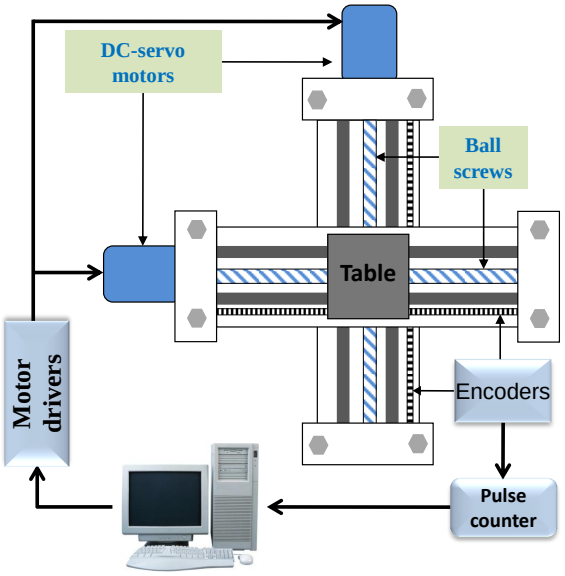

FIGURE 2.1: Typical lead-screw feed drive system

modeling and control design; Section 2.3 provides simulation and experimental results to validate the effectiveness of the proposed method; and lastly, Section 2.4 gives the concluding remarks.

2.2 System Modeling and Control Design

2.2.1 System modeling

This study considered a typical lead-screw feed drive system (Fig. 2.1). A DC-servo motor, commonly used in industrial applications was used to drive the feed drive system. The feed drive system dynamics was generally represented by the following decoupled

second-order system:

$$\begin{aligned} &M\ddot{x} + C\dot{x} + d = f, \\ &M = \text{diag}\,(m_i)\,,\ C = \text{diag}\,(c_i)\,,\ i = 1,\ 2, \\ &f = [f_1,\ f_2]^T\,,\ d = [d_1,\ d_2]^T\,,\ x = [x_1,\ x_2]^T, \end{aligned} \tag{2.1}$$

where M and C are the table mass and the viscous friction coefficient matrices, respectively. d, f, and x are the disturbances to the system, driving forces, and positions of the i^{th} drive axis, respectively. Each drive axis had an attached servo motor providing a rotational motion and transmitting it to a lead screw via coupling. The lead-screw rotation was then transformed into a linear movement of the table by the feed drive axes. The corresponding motor dynamics is represented as follows:

$$\begin{aligned} &N\ddot{\theta} + H\dot{\theta} + \tau = K_t i_a, \\ &N = \text{diag}\,(n_i)\,,\ H = \text{diag}\,(h_i)\,,\ K_t = \text{diag}\left(k_{t_i}\right), \\ &\theta = [\theta_1,\ \theta_2]^T\,,\ \tau = [\tau_1,\ \tau_2]^T\,,\ i_a = \left[i_{a_1}, i_{a_2}\right]^T, \end{aligned} \tag{2.2}$$

where N, θ, and H denote the inertia matrix, rotational angle vector, and viscous friction coefficient matrix of the motors, respectively. τ, K_t, and i_a are the torque vector required to drive the feed drive system, torque constant matrix, and input current vector, respectively. The relationships between the forces f, torque τ, positions x, and angles θ are represented by the following equation:

$$f_i = \frac{2\pi\tau_i}{p_i},\ x_i = \frac{p_i\theta_i}{2\pi}, \tag{2.3}$$

TABLE 2.1: System parameters

Axis	m_i (kg)	c_i (Nsmm^{-1})	n_i (kgm^2)	h_i (Nms/rad)
1	8.0	102.48	0.05	0.31
2	2.5	140.90	0.05	0.31

where p_i is the pitch of the i^{th} drive axis. Equations (2.1), (2.2), and (2.3) lead to the following plant dynamics:

$$\begin{aligned} u &= J_e\ddot{x} + B_e\dot{x} + d, \\ J_e &= \text{diag}\left(\frac{4\pi^2 n_i + m_i p_i^2}{p_i^2}\right), \\ B_e &= \text{diag}\left(\frac{4\pi^2 h_i + c_i p_i^2}{p_i^2}\right), \\ u &= K_\mu i_a,\ K_\mu = \text{diag}\left(\frac{2\pi k_{t_i}}{p_i}\right), \end{aligned} \tag{2.4}$$

where J_e and B_e are the equivalent inertia and friction coefficients representing the combined linear and rotary coefficients, respectively. Table 2.1 lists the actual system parameters. The tracking error of the system is given as follows:

$$\begin{aligned} e &= x_r - x, \\ e &= [e_1,\ e_2]^T,\ x_r = [x_{r_1},\ x_{r_2}]^T, \end{aligned} \tag{2.5}$$

where x_r is the desired position vector. The error dynamics of the feed drive system can be written as follows:

$$\ddot{e} = \ddot{x}_r - J_e^{-1}(u - d - B_e\dot{x}). \tag{2.6}$$

The state space representation of the above-mentioned system is presented as follows:

$$
\begin{aligned}
&\dot{z} = Az + bu - \tilde{d},\\
&y = cz,\\
&z = [z_1,\ z_2,\ z_3,\ z_4]^T, c = [1,\ 1,\ 0,\ 0],\\
&A = \begin{bmatrix} 0 & 0 & 1 & 0 \\ 0 & 0 & 0 & 1 \\ 0 & 0 & -\frac{B_{e1}}{J_{e1}} & 0 \\ 0 & 0 & 0 & -\frac{B_{e2}}{J_{e2}} \end{bmatrix}, b = \begin{bmatrix} 0 & 0 \\ 0 & 0 \\ \frac{1}{J_{e1}} & 0 \\ 0 & \frac{1}{J_{e2}} \end{bmatrix}, \tilde{d} = \begin{bmatrix} 0 \\ 0 \\ \frac{d_1}{J_{e1}} \\ \frac{d_2}{J_{e2}} \end{bmatrix},
\end{aligned}
\tag{2.7}
$$

where states z_1 and z_2 represent the positions of the feed drive and are measured using rotary encoders of equivalent resolution of 0.025μm. A low-pass filter with a cutoff frequency ω_f of 75 Hz is employed to estimate the states z_3 and z_4 from z_1 and z_2 respectively. $\tilde{d} = \left[\tilde{d}_1,\ \tilde{d}_2,\ \tilde{d}_3,\ \tilde{d}_4\right]^T$ is assumed to be matched (i.e. it lies in the space range of the input matrix b).

2.2.2 Assumptions

The following assumptions ware considered herein for controller design:

1. The nominal parameters of J_e and C_e are known.

2. Positions x_1 and x_2 and velocities $\dot{x}_1$ and $\dot{x}_2$ are measurable.

3. d is unknown, but bounded.

4. The reference signal for x and $\dot{x}$, x_r and $\dot{x}_r$, are given.

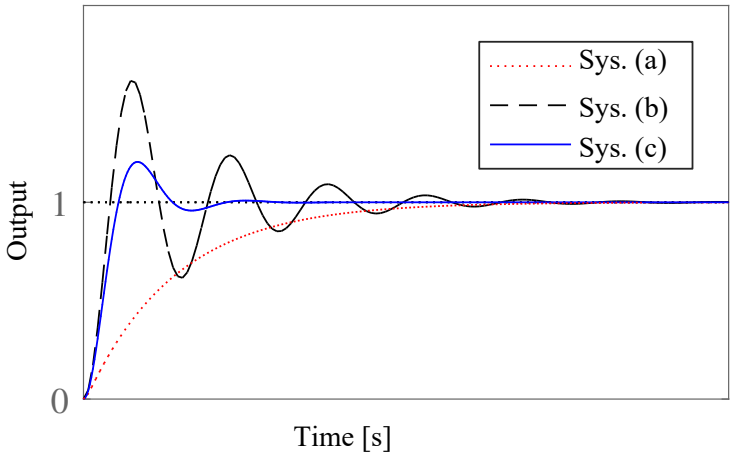

FIGURE 2.2: System response with different damping ratios. System (a) with high damping ratio, System (b) with low damping ratio, System (c) with nonlinear damping ratio.

2.2.3 Sliding Surface Design and its Stability Analysis

A nonlinear sliding surface was employed to improve the control performance [76]. The dynamic system response solely depends on its damping ratio. A common second-order system with a different damping ratio can be used to explain this. Fig. 2.2 illustrates the step response of three different second-order systems with different damping ratios. System (a) has a large damping ratio; therefore, the system response is very slow with a larger tracking error and a smaller energy consumption. System (b) has a small damping ratio; hence, the system response is very fast with a large overshoot that increases the energy consumption. System (c) is a combination of the two previous systems. A smaller damping ratio is assigned in the beginning to achieve a fast response. To prevent a high overshoot, a larger damping ratio is assigned when the output value is close to the reference. The advantage of this combination is that it reduces the energy consumption while maintaining the motion accuracy in most electromechanical and robotic systems used all over the world day and night. This subsection considers the design of the adaptive

sliding mode controller with a nonlinear sliding surface for the lead-screw feed drive system. The damping ratio of the closed-loop system can be changed from a low initial value to a high final value using a nonlinear sliding surface. The low initial value of the damping ratio results in a quick response, whereas the subsequent high damping ratio avoids an overshoot to minimize the energy consumption. The following nonlinear sliding surface is considered herein on the basis of the system dynamics in (2.7) [76]:

$$s = \begin{bmatrix} A & I \end{bmatrix} \begin{bmatrix} e \\ \dot{e} \end{bmatrix}, \tag{2.8}$$

$$A = \text{diag}(\lambda_i + \psi_i \gamma_i),$$

where λ_i is the linear term of the sliding surface. This value was chosen such that dominant poles have a low damping ratio. γ_i is a positive definite matrix used to adjust the damping ratio and ψ_i is a non-negative differentiable function that depends on the output and desired velocity. It is also used to change the damping ratio of the system from its low initial value to a high final value as the output changes from its low initial value to the desired value. The choice of ψ_i is not unique. Function ψ_i should have the following properties:

1. The function should vary from 0 to a certain positive value β_i because the error varies from a large value to zero when changing the system damping ratio.

2. The function should be differentiable with respect to x.

ψ_i is defined herein as follows based on the nonlinear function presented in [37] for a step-type reference trajectory:

$$\psi_i = \frac{\beta_i}{(1 - \exp(-1))} \left\{ \exp\left[\left(\frac{\dot{x}_i}{\dot{x}_{r_i}} \right)^2 - 1 \right] - \exp(-1) \right\}, \tag{2.9}$$

$$\dot{x}_{r_i} \neq 0,$$

where β_i is the positive turning parameter used to adjust the weight of the nonlinear term. The magnitude of ψ_i becomes small if the system output is far from the desired point. This provides a low damping ratio and speeds up the system response.

The system can be forced to the sliding surface by applying some control law, which will be presented later. On the sliding surface, (i.e., when $s = 0$), we have

$$\dot{e} = -Ae, \tag{2.10}$$

where A is not a constant matrix, it includes the time variant parameter ψ_i.

The following Lyapunov function candidate for the system in Eq. (2.10) is considered to verify the stability of the proposed sliding dynamics:

$$V = \frac{1}{2} e e^T. \tag{2.11}$$

Substituting (2.10) into the time derivative of V leads to

$$\dot{V} = -eAe^T. \tag{2.12}$$

A is a positive definite matrix; hence, we have $\dot{V} \leq 0$, which ensures system stability during the ideal sliding mode.

2.2.4 Controller Design and its Stability Analysis

In this section, the control law is designed to enforce the system in Eq. (2.4) to move from any initial conditions to the desired sliding surface and thereafter remain on it. The following control law was designed assuming that the reference position, velocity, and

acceleration are given and considering the feed drive dynamics:

$$\begin{aligned} u &= J_e \left\{ \ddot{x}_r + A\dot{e} + \hat{K}s - Be \right\} + Q\text{sign}(s) + B_e\dot{x}, \\ B &= \text{diag}\left(\frac{d\psi_i}{dt}\gamma_i \right),\ \hat{K} = \text{diag}\left(\hat{k}_i \right), \end{aligned} \tag{2.13}$$

where $\hat{K}(0) > 0$ is the adaptive gain matrix and $Q \in R^{2\times 2}$ is a diagonal matrix with diagonal elements q_i chosen from the maximum bound of the uncertainty as follows:

$$q_i \geq \max(d_i). \tag{2.14}$$

The adaptive law was chosen as follows based on the idea in Ref. [87]:

$$\dot{\hat{k}}_i = \begin{cases} \bar{k}_i |s_i| \text{sign}(|s_i| - \epsilon_i) & \text{if } \hat{k}_i > \mu_i \\ \mu_i & \text{otherwise} \end{cases}, \tag{2.15}$$

where ϵ_i, μ_i, and $\bar{k}_i$ are very small positive constants. The parameter μ_i was introduced to obtain positive values for $\hat{k}_i$. For discussion, proof, and clarity, and without loss of generality, one supposes that $\hat{k}_i(t) > \mu_i$ for all $t > 0$. Suppose that $|s_i(t)| > \epsilon_i$, it follows that $\hat{k}_i$ is increasing and there exists a time t_1 (see Fig. 2.3) such that from $t = t_1$, gain $\hat{k}_i$ is large enough to make the sliding variable s_i decreasing. Then, it yealds that, in a finite time t_2 (Fig. 2.3), $|s_i| < \epsilon_i$. It yields that gain $\hat{k}_i$ is decreasing from t_2, gain $\hat{k}_i$ being at a maximum value at $t = t_2$. From the $\hat{k}_i$-dynamics, it yields that there exists a time instant $t_3 > t_2$ (Fig. 2.3) such that $\hat{k}_i$ is not large enough to counteract perturbations and uncertainties as it is decreasing. It yields that there exists a time instant $t_4 > t_3$ such that $|s_i(t_4)| > \epsilon_i$. The process then restarts from the beginning.

In summary, once the sliding mode is established with respect to s_i, the proposed gain adaption law (2.15) lets the gain $\hat{k}_i$ decrease (while $|s_i| < \epsilon_i$). In other words, the gain

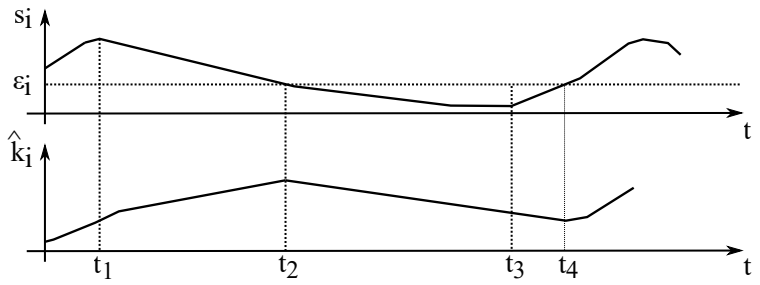

FIGURE 2.3: Scheme describing the behaviour of s_i (top) and $\hat{k}_i$ (bottom) versus time.

$\hat{k}_i$ will be kept at the smallest level that allows a given accuracy of the sliding surface stabilization. This adaption law maintains an adequate gain magnitude with respect to disturbances.

For asymptotic stability and to force the tracking error unto the desired sliding surface as $t \to \infty$, the time derivative of the following Lyapunov candidate must be negative:

$$V_i = \frac{1}{2} s_i^2 + \frac{1}{2} (\hat{k}_i - k_i^*)^2, \tag{2.16}$$

where k_i^* is an upper bound of the control gain $\hat{k}_i$ such that

$$\hat{k}_i \leq k_i^*.$$

The time derivative of the Lyapunov function in (2.16) is written as follows:

$$\dot{V}_i = s_i \dot{s}_i + \left(\hat{k}_i - k_i^* \right) \dot{\hat{k}}_i. \tag{2.17}$$

From the time derivative of the sliding surface in (2.8) and the adaption rule for the controller gain $\hat{k}_i$ in (2.15), the time-derivative of V_i becomes

$$\begin{aligned}\dot{V}_i =& s_i \left\{ \left(\lambda_i - \psi_i \gamma_i\right) \dot{e}_i + \ddot{e}_i - \frac{d\psi_i}{dt}\gamma_i e_i \right\} \\ &+ \left(\hat{k}_i - k_i^*\right) \bar{k}_i |s_i| \text{sign}(|s_i| - \epsilon_i). \end{aligned} \tag{2.18}$$

Substituting Eqs. (2.6) and (2.13) into (2.18) leads to the following:

$$\begin{aligned}\dot{V}_i =& s_i \left\{ -\hat{k}_i s_i - q_i \text{sign}(s_i) + d_i \right\} + \\ & \left(\hat{k}_i - k_i^*\right) \bar{k}_i |s_i| \text{sign}(|s_i| - \epsilon_i), \\ =& |s_i| \left\{ -\hat{k}_i - q_i + d_i + \left(\hat{k}_i - k_i^*\right) \bar{k}_i \text{sign}(|s_i| - \epsilon_i) \right\}. \end{aligned} \tag{2.19}$$

We considered herein the following two cases for the stability analysis:

• **Case 1** When $|s_i| \geq \epsilon_i$ as in the first condition in Eq. (2.15), $\left(\hat{k}_i - k_i^*\right) \bar{k}_i \text{sign}(|s_i| - \epsilon_i)$ is non-positive, and

$$\dot{V}_i < 0. \tag{2.20}$$

• **Case 2** When $|s_i| < \epsilon_i$ as in the second condition in Eq. (2.15), $\left(\hat{k}_i - k_i^*\right) \bar{k}_i \text{sign}(|s_i| - \epsilon_i)$ is non-negative. By choosing q_i as

$$q_i \geq \left(\hat{k}_i - k_i^*\right) \bar{k}_i + d_i, \tag{2.21}$$

we obtained $\dot{V}_i < 0$, and the system stability is guaranteed.

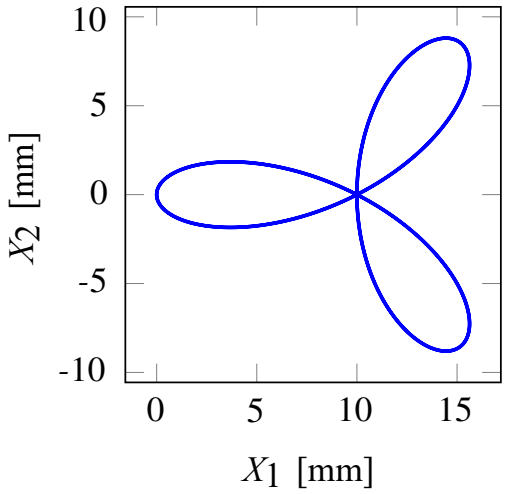

FIGURE 2.4: Reference trajectories

2.3 Simulation and Experiment

To validate the effectiveness of the proposed method, simulation and experiment were conducted. A trifolium trajectory in Eq. (2.22) and Fig. 2.4 was used. The results were compared to those of the sliding mode control without adaption. The performance of the proposed method (i.e., ASMC) was also compared to that in Ref. [85] through a simulation:

$$x_{r_1} = r^* \cos\left(\frac{2\pi t}{T}\right),\ x_{r_2} = r^* \sin\left(\frac{2\pi t}{T}\right),$$

$$r^* = r \cos\left(\frac{2\pi t}{T}\right)\left\{4\sin^2\left(\frac{2\pi t}{T}\right) - 1\right\}, \tag{2.22}$$

where r is the radius, and T is the total time to complete the trajectory. Table 2.2 presents the controller parameters. These parameters were used for both the simulation and the experiment.

TABLE 2.2: Controller parameters

Control	λ_i (s^{-1})	γ_i (s^{-1})	β_i	q_i (ms^{-2})	k_i (s^{-1})
ASMC	40	1.8	10	0.3	variable
SMC	40	1.8	10	0.3	80

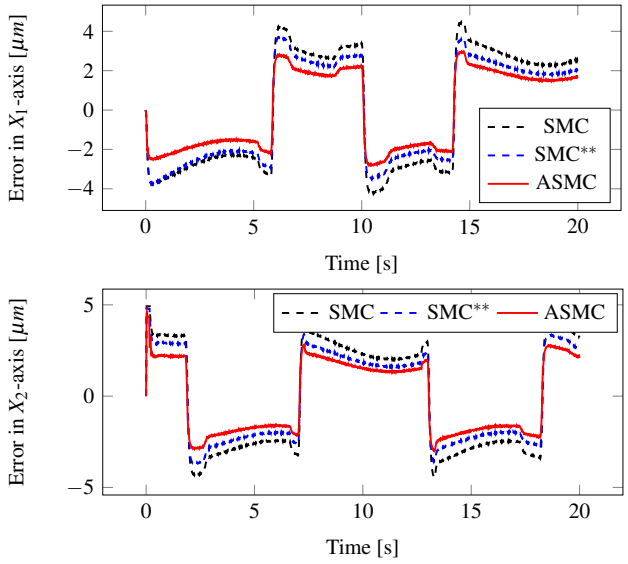

FIGURE 2.5: Simulation results of tracking performance

2.3.1 Simulation Results

Fig. 2.5 shows the simulation results of the tracking performance. The initial tracking error was large because reference trajectory was implemented by a typical G-code that generates constant velocity motion profiles. However, ASMC achieved a better tracking performance than SMC and reduced the average tracking error by 33 %. The SMC** in Fig. 2.5 depicts the tracking error results when the gain adaption law $K_c = \int \rho S_m^2 dt$ in [85] was used. The values of ρ and the upper bound for K_c were set to 0.8 and 100 s^{-1}, respectively. ASMC yielded a better performance over SMC** because the proposed adaptive law varied according to the tracking error, while that in [85] remained at the upper limit (Fig. 2.6). Table 2.3 summarizes the simulation results.

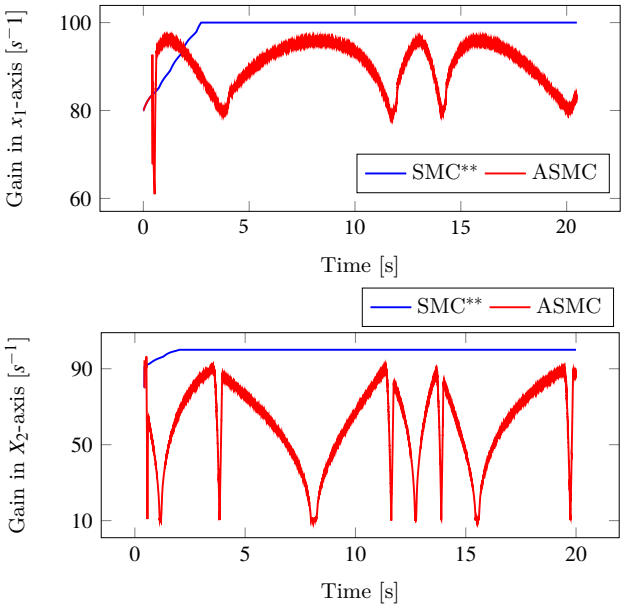

FIGURE 2.6: Adaptive gain K_c

TABLE 2.3: Summary of simulation results

Controller	Tracking error [μm]			
	Maximum		Mean	
	X_1-axis	X_2-axis	X_1-axis	X_2-axis
SMC	4.46	4.18	0.34	0.50
ASMC	2.96	2.82	0.23	0.33

2.3.2 Experimental Results

A typical biaxial lead-screw feed drive system (Fig. 2.7) was used for the experiment. The feed drive system comprised a table coupled by two lead-screw drives driven by DC-servo motors connected to each drive axis. Rotary encoders (equivalent resolution: 0.025 μm) were used to measure the actual table position. The velocity signal was calculated by a numerical differentiation of the measured position. The control law was implemented using the C^{++} program on a personal computer (OS: Windows XP, CPU: 2 GHz) with 5 ms sampling time. We employed timer on a counter board of 24-bit up/down counters to

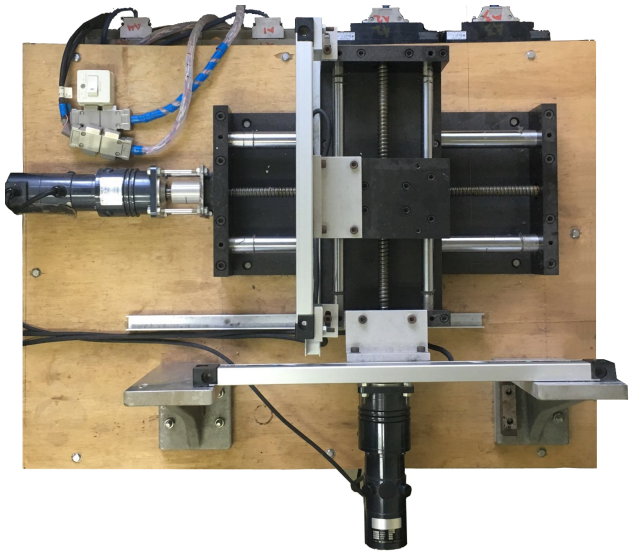

FIGURE 2.7: Biaxial feed drive system

provide a fixed sampling period in a Windows XP environment.

An experiment was conducted for the trifolium trajectory to confirm the effectiveness of the proposed method in performance enhancement and energy saving. In the first case, the aim was to confirm the effectiveness of the proposed approach in reducing the tracking error by comparing the performance of ASMC to SMC. In this comparison, the same parameters were used for both controllers to conduct a fare comparison except for gain $\hat{K}$, which varied for the case of ASMC. Note, however, that the initial gain $\hat{K}$ for ASMC was set to the same value of that of SMC. The controllers' parameters in Table 2.2 were used in the experiment, similar to the simulation. The electrical energy consumption was measured by a power Hi-tester HIOKI 3334 AC/DC. The results were then compared to those of SMC with no adaption. The same experiment was repeated for five times to ensure the repeatability of the proposed method. Fig. 2.8 shows the consumed electrical energy for five trials. In all the trials, the proposed controller (i.e., ASMC) consumed lesser energy than SMC. ASMC reduced the energy consumption by 3.4 % for the trifolium trajectory. The experimental results for the tracking errors and the control input voltages

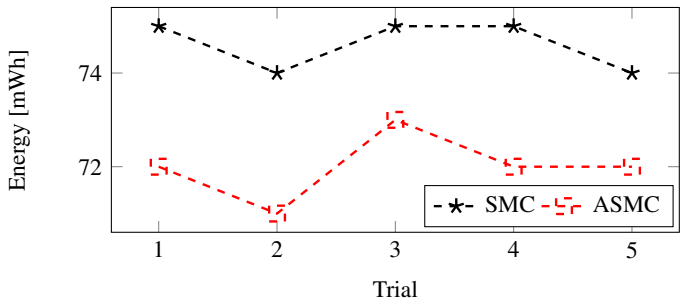

FIGURE 2.8: Experimental results of energy consumption

ware taken from 1 s after the start of the experiment. Fig. 2.9 illustrates the tracking error results showing that ASMC achieved a better tracking performance compared to SMC by reducing the average tracking error by 50 % and 43.7 % in the X_1 and X_2 drive axes, respectively. Fig. 2.10 displays the maximum absolute values of the tracking errors for five trials. The input voltage is shown in Fig. 2.11, where the proposed method had a smoother input voltage than SMC, which had more chattering, especially in the X_1-axis. Tables 2.4 and 2.5 list the summary of the experimental tracking performance and energy consumption results, respectively. In addition, the control input variance was calculated by the following equation:

$$\sigma_i^2 = \frac{\sum_{j=1}^{N} u_{ij}^2}{N} - \bar{u}_i^2, \tag{2.23}$$

where σ_i is the standard deviation; u_{ij} is the control input value at the j^{th} sampling instant of the i^{th} drive axis; $\bar{u}_i$ is the mean of all the control input values of the i^{th} drive axis; and N is the total number of sampling instants. Fig. 2.12 shows the control input variance showing that the proposed approach achieved a smaller control input variance than SMC in both axes. These results clearly showed that ASMC achieved a better performance than SMC. In the second case, we confirmed the effectiveness of the proposed method in saving energy under a similar tracking performance using the same trajectory. The

linear term λ_i of the sliding surface was increased from $40\,s^{-1}$ to $80\,s^{-1}$ to achieve similar tracking performances for both SMC and the proposed ASMC. Hereinafter, the SMC with

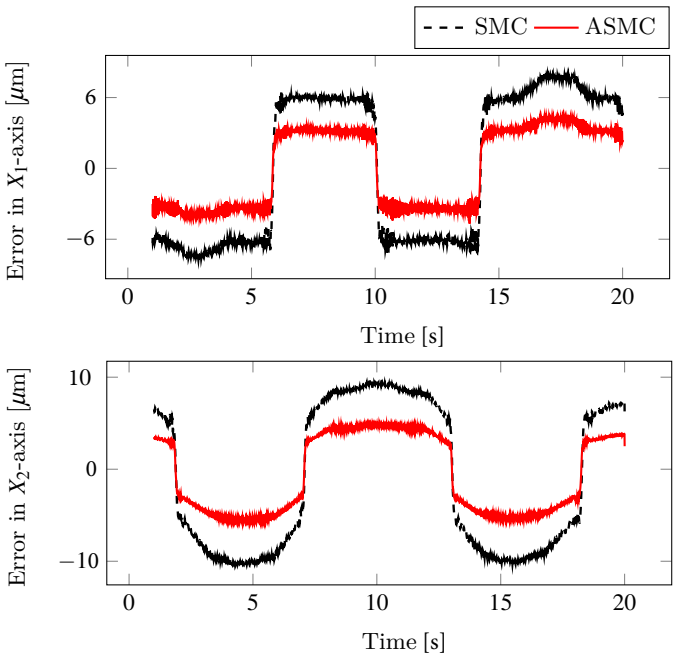

FIGURE 2.9: Experimental results of tracking performance

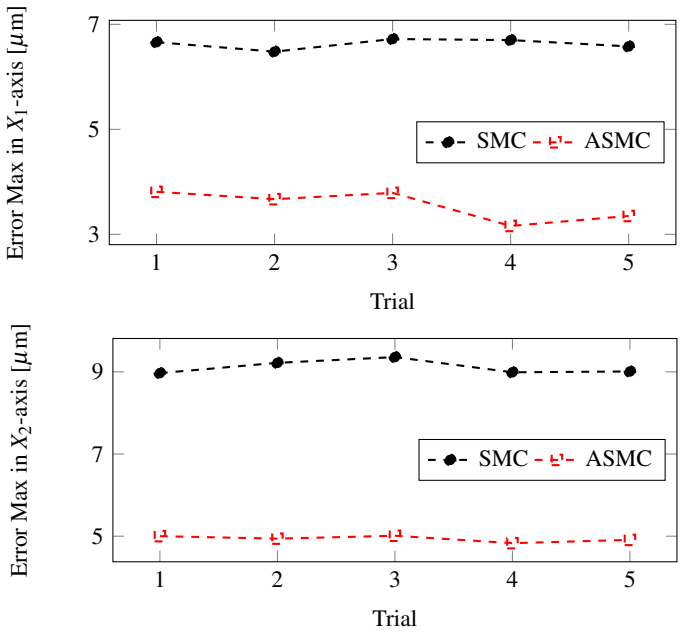

FIGURE 2.10: Experimental results of maximum tracking error

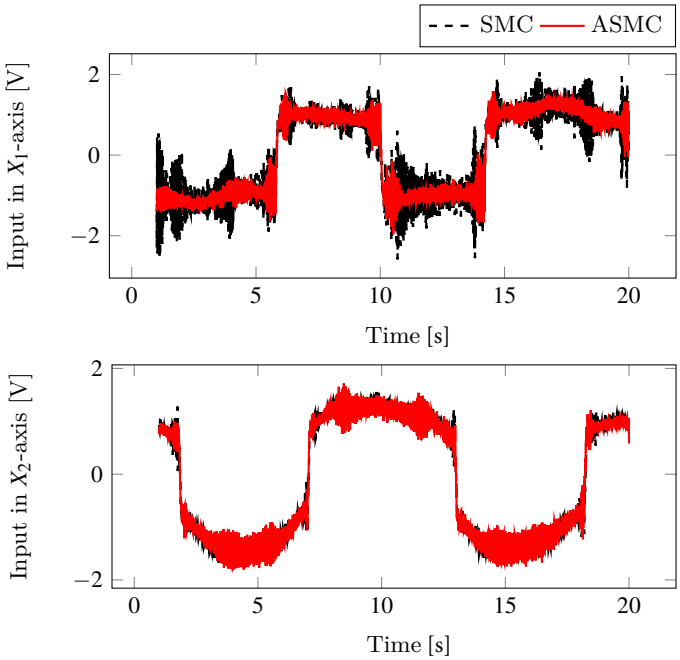

FIGURE 2.11: Experimental results of input voltage

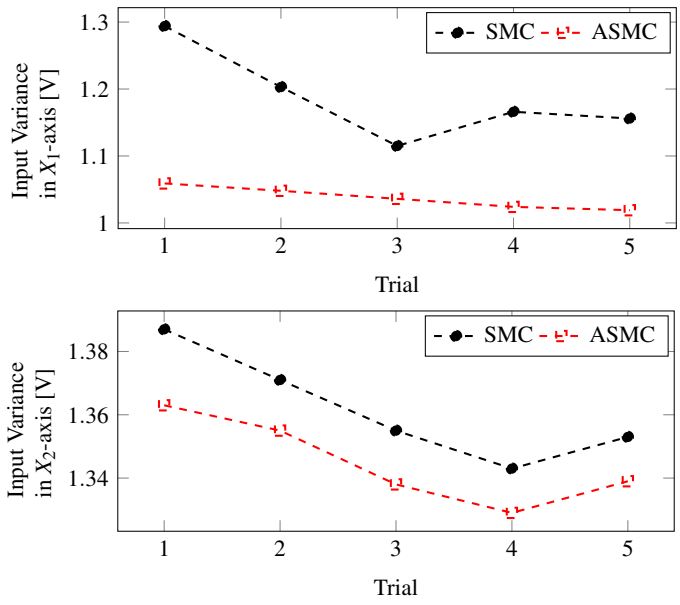

FIGURE 2.12: Experimental results of input variance

a raised linear-term gain is referred to as the SMC*. The experiment was repeated for five times. Subsequently, the results were compared to those obtained by the proposed method.

TABLE 2.4: Summary of experimental tracking performance results

Controller	Tracking error [μm]			
	Maximum		Mean	
	X_1-axis	X_2-axis	X_1-axis	X_2-axis
SMC	6.72	9.36	0.16	1.28
ASMC	3.81	5.01	0.08	0.72

TABLE 2.5: Summary of experimental input variance and energy consumption results

Controller	Input variance [V]		Energy consumption [mWh]
	Mean		Mean
	X_1-axis	X_2-axis	
SMC	1.30	1.36	74.6
ASMC	1.04	1.19	72.0

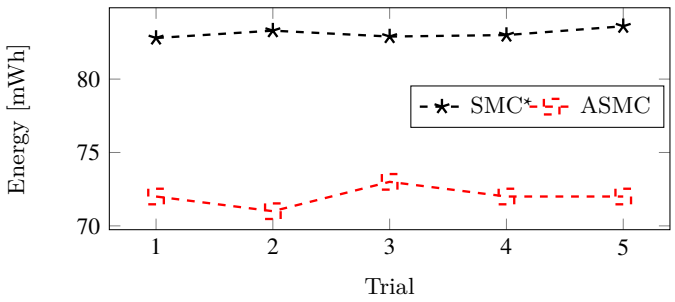

FIGURE 2.13: Experimental results of energy consumption under similar tracking performance

The total energy consumed by SMC* was increased from the average of 74.6 to 83.1 mWh by increasing the linear-term gain. Fig. 2.13 shows the energy results for the five trials, in which the two controllers had a similar tracking performance, and SMC consumed more energy. Fig. 2.14 depicts the tracking performance for the two cases; case 1 for similar parameters and case 2, where λ_i was increased in SMC to achieve tracking performance similar to that of ASMC. Fig. 2.15 illustrates the corresponding input signals, where the control input for SMC had more chattering than that of ASMC. The control input variance

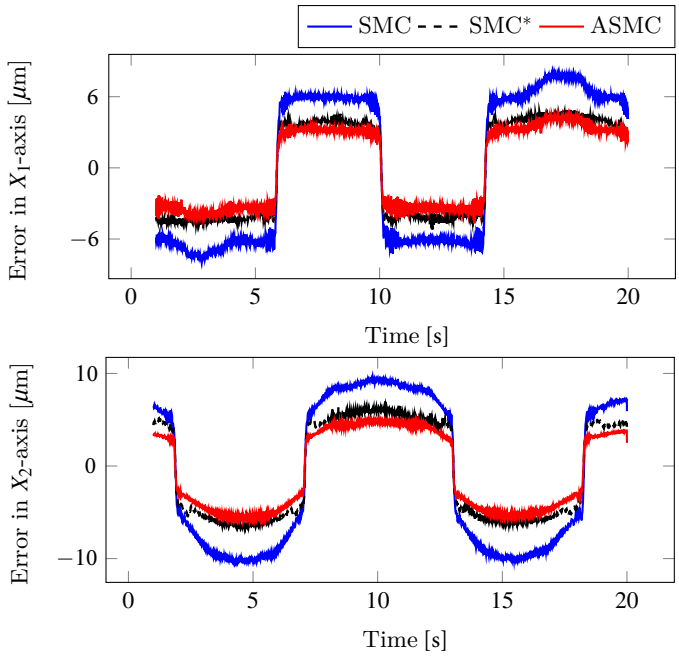

FIGURE 2.14: Experimental results of tracking error under similar tracking performance

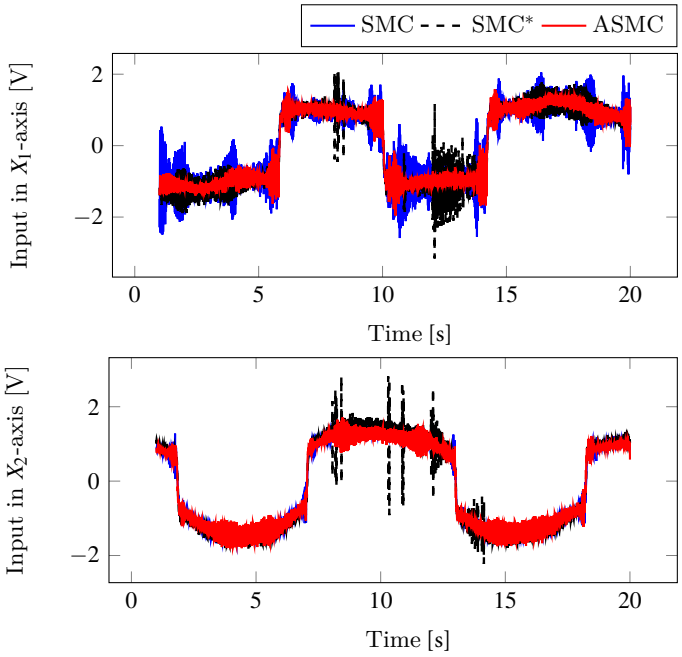

FIGURE 2.15: Experimental input voltage under similar tracking performance

for SMC* increased from 1.14 to 1.16 V in the X_1-axis, and from 1.28 to 1.47 V in the X_2-axis compared to SMC. The proposed method achieved smaller input variances of 1.04 V and 1.19 V in the X_1 and X_2-axes, respectively.

2.4 Conclusion

This study, proposed adaptive sliding mode control with a nonlinear sliding surface for the precision motion and energy saving of feed drive systems. Simulations and experiments were conducted to demonstrate the effectiveness of the proposed method in terms of energy saving and tracking performance enhancement in feed drive systems. The results were compared to those of the sliding mode control without adaption to evaluate the performance of the proposed method. In summary, the results showed that the energy consumption, tracking error, and control input variance of the proposed controller were smaller than those of the nonadaptive sliding mode control. The proposed controller could reduce the consumed energy by 3.4 % for a trifolium trajectory. In addition, the tracking performance could be enhanced by reducing the maximum tracking error by 45 %. Moreover, the proposed method achieved a smaller control input variance by 12.6 % compared to SMC. We used a typical lead screw-based X-Y table to verify the method effectiveness; thus, the proposed controller can be widely applied in various industrial systems.

Chapter 3

Adaptive Sliding Mode Controller Design with a Feedforward Compensator for the Energy-efficient and High-precision Motion of Feed Drive Systems

3.1 Introduction

Feed drive systems are among the most dominating motion components in the production and manufacturing industries because of their wide range of use (e.g., in multi-axis motions) [88–92]. The growing demand for precise products poses the need for high-speed production systems with a higher accuracy. In most cases, feed drive systems operate around the clock; therefore, they are among the major consumers of the industrial energy supply. Energy consumption is one of the reasons for using lighter components in feed drive systems. While high-speed motion is preferred, it causes vibration in light systems,

high-energy consumption, and a poor tracking performance. As explained in [74], [93], and [90], the control performance greatly depends on the systems vibration, unmodeled uncertainties, and external disturbances.

Many studies have focused on the positioning and tracking control of servomotors, which are widely used in motion control applications because of their basic advantages, such as high power density and torque-to-inertia ratio, high performance and efficiency, and low noise [94, 95]. Accordingly, classical and modern control techniques, such as sliding mode control (SMC), adaptive control, dynamic friction compensation methods, and back-stepping control, have been widely applied [94, 96–100]. On the contrary, applications using feed drive systems commonly use repetitive and iterative learning controls under the assumption that these systems are used for mass productions [90]. However, many feed drive applications are not repetitive; thus, considering control strategies for general applications is indispensable.

Ref. [101] employed a practical method, called the robust integral of the sign of the error controller and synthesized it with a continuous differentiable friction model to achieve the high-accuracy motion of a DC motor. A model-based desired compensation was employed in the controller to reduce or control the chattering and sensitivity to noise during application. As a result, the tracking performance can be enhanced.

Linear motors have recently been increasingly applied in high-speed machine tools. However, they are more expensive and sensitive to disturbance because of the direct conversion of the motor current to the driving force without a motion transmission gear. They also face the synchronization problem in practical applications. The research works of [102] and [103] proposed effective methods for eliminating the synchronization problem. In contrast, ball-screw feed drives are often used in machine tools because of their advantages of low costs, high stiffness against cutting forces, and robustness to disturbances and table load variations due to their high gear ratio. Some machining tasks require high cutting

forces, consistency, and stability, and for cases involving these requirements, a ball-screw drive is the best solution. Therefore, we believe that it is inevitable to continue conducting research on ball-screw feed drive systems.

Robust controllers, such as SMC, have been proven to provide a reasonable performance under the effect of external disturbance and system uncertainties [55, 70–74, 104]. Apart from its simplicity in design, SMC is robust against perturbation and invariant to matched uncertainties. Other SMC variants include adaptive sliding mode control (ASMC) and nonlinear sliding mode control which are more flexible and offer a higher tracking performance compared to the traditional SMC [105, 106].

Meanwhile, model-based approaches (e.g., feedforward friction compensator) are applied to cancel out the effect of the estimated friction force. However, friction sources generally have complex nonlinear properties; thus, finding a perfect model is difficult, and the performance exclusively depends on the veracity of the estimated model [107, 108]. Ref. [109] derived a continuously differentiable nonlinear friction model by modifying the LuGre model, which is piecewise continuous, and proposed a controller to take care of the parametric uncertainties along with the nonlinear friction compensation. Despite the promising performance of the abovementioned approaches, enhancing both the tracking performance and the energy consumption of feed drive systems is indispensable.

Feed drive systems generally include various nonlinear uncertainties, such as backlash, friction forces, modeling errors, and parameter variation, among others. Preloading is applied in ball-screw feed drive systems and can be described as the tension induced on the ball-screw drive when no external loads are applied. The additional load aims to eliminate backlash and increase the position accuracy of the ball-screw during operation [110]. Backlash is not a big problem in ball-screw drive systems because of preloading. Friction, however, is the main disturbance. Some studies focused on the control of a specific type of uncertainty. For example, Ref. [111] proposed a joint toque control for

backlash compensation in a two-inertia system, where the backlash was modeled as a dead zone. However, the complete cancellation of specific uncertainties requires having accurate models. In practice, modeling each uncertainty, which may exist in a plant, is impractical. Therefore, designing a controller that is robust and can automatically cancel out the effect of these uncertainties without focusing on its specific type is inevitable.
This study primarily aims to improve the tracking performance by explicitly considering the uncertainty dynamics. Accordingly, a nonlinear SMC with a feedforward compensator for system uncertainties is applied. As stated in [112], the feedforward compensator refers to a modeled system with assumed uncertainty dynamics. The controller is designed by taking the difference between a reference model and the real system. The proposed method enhances the tracking performance of feed drive systems while maintaining the required energy. Adding another compensator for a specific uncertainty is expected to not degrade the proposed controller's performance, but enhance it. The system stability was analyzed and confirmed through the Lyapunov stability theory. Its convergence to the sliding surface was also assured.

3.2 System Dynamics

Feed drive systems have many configurations; therefore, a typical biaxial setup, which is also referred to as the X-Y table, is considered herein. Its dynamics can be represented in a decoupled format as follows [113]:

$$\begin{aligned} &M\ddot{x} + C\dot{x} + L\text{sign}(\dot{x}) + d = f, \\ &M = \text{diag}\,(m_i)\,,\ C = \text{diag}\,(c_i)\,,\ L = \text{diag}\,(l_i)\,,\ i = \{1,2\}, \\ &f = [f_1,\ f_2]^T\,,\ d = [d_1,\ d_2]^T\,,\ x = [x_1,\ x_2]^T, \end{aligned} \tag{3.1}$$

where m_i, c_i, and l_i represent the mass, viscous friction coefficient, and Coulomb friction force for each drive axis i, respectively. The input (driving force), external disturbance, and position of each drive axis are denoted as f_i, d_i, and x_i, respectively. Note that the drive axes are driven by servo motors that are mechanically coupled to the system; thus, the dynamics of these motors are included in the system. The dynamics of the attached motors is defined as follows [105]:

$$\begin{aligned} &N\ddot{\theta} + H\dot{\theta} + \tau = K_t i_a, \\ &N = \text{diag}\left(n_i\right),\ H = \text{diag}\left(h_i\right),\ K_t = \text{diag}\left(k_{t_i}\right), \\ &\theta = \left[\theta_1,\ \theta_2\right]^T,\ \tau = \left[\tau_1,\ \tau_2\right]^T,\ i_a = \left[i_{a_1}, i_{a_2}\right]^T, \end{aligned} \tag{3.2}$$

where $n_i, \theta_i, h_i, \tau_i, k_{ti}$ and i_{ai} are the inertia, angular position, viscous friction coefficient, output torque, torque constant, and input electric current for each motor i, respectively. The plant dynamics can be represented as follows:

$$\begin{aligned} &u = J_e\ddot{x} + B_e\dot{x} + L\text{sign}(\dot{x}) + d, \\ &J_e = \text{diag}\left(\frac{4\pi^2 n_i + m_i p_i^2}{p_i^2}\right), \\ &B_e = \text{diag}\left(\frac{4\pi^2 h_i + c_i p_i^2}{p_i^2}\right), \\ &u = K_\mu i_a,\ K_\mu = \text{diag}\left(\frac{2\pi k_{t_i}}{p_i}\right), \end{aligned} \tag{3.3}$$

where p refers to the pitch of the ball screws that converts the motors' angular motion to the linear motion of the drive axes. The nominal values of J_e and B_e are assumed to be known.

3.3 Controller Design

We define the positional tracking error of the system as follows prior to the controller design:

$$\begin{aligned} e &= x_r - x, \\ e &= [e_1,\ e_2]^T,\ x_r = [x_{r_1},\ x_{r_2}]^T, \end{aligned} \tag{3.4}$$

where x_r is the reference position. From (3.3), the error dynamics can be written as:

$$\ddot{e} = \ddot{x}_r - J_e^{-1}\left\{u - B_e\dot{x} - L\text{sign}(\dot{x}) - d\right\}. \tag{3.5}$$

The proposed control structure comprises the reference plant model, a real plant, and the uncertainty dynamics compensator, as shown in the block diagram (Fig. 3.1). The following linear equation is considered as the reference model

$$\begin{aligned} \bar{u} &= J_e\dddot{\bar{x}} + B_e\ddot{\bar{x}}, \\ \bar{x} &= [\bar{x}_1,\ \bar{x}_2]^T, \end{aligned} \tag{3.6}$$

where $\bar{x}_i$ and $\bar{u}$ are the position of the i^{th} drive axis and the input vector to the reference model, respectively. The control input to the real plant is defined as $u = \bar{u} + v$, where v is the compensator for the uncertainty dynamics.

3.3.1 Sliding Mode Controller Design

In designing a sliding mode controller, we first considered selecting a nonlinear sliding surface that will ensure that the system can effectively track the reference trajectory. The sliding surface must guarantee that the control systems are asymptotically stable. A control

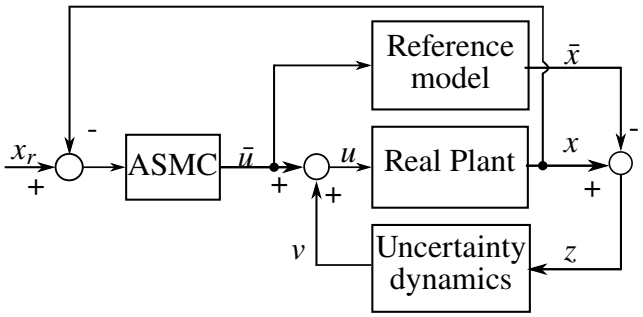

FIGURE 3.1: Block diagram of the proposed control system

law is then selected to drive the system to follow the reference trajectory. To confirm that the control system is stable, the selected control law must ensure that the error dynamics is exponentially decaying with time. One must have a system that can respond as fast as possible without having overshoots. To do that, a variable damping ratio is applied, such that a low damping ratio is applied at the initial stage to assist the fast response and gradually increased to minimize the overshoots. A variable damping ratio allows for a better tracking performance while minimizing the energy consumption. The following nonlinear sliding surface was applied herein [76]

$$\bar{s} = \begin{bmatrix} A & I \end{bmatrix} \begin{bmatrix} e \\ \dot{e} \end{bmatrix},$$

$$A = \text{diag}(\lambda_i + \psi_i \gamma_i), \tag{3.7}$$

where λ_i is the linear term for the sliding surface. The linear term was selected by ensuring that predominant poles had a small damping ratio. γ_i is a positive linear term assisting the adjustment of the damping ratio. ψ_i is a non-negative differentiable nonlinear function of the error. This function was upper-bounded, such that $\psi_i \leq \psi_{max_i}$, and its role was to facilitate the adjustment of the system's damping ratio and change it. The system output varied from its initial value, ψ_i thereby gradually increasing the damping ratio. The

following ψ_i is considered herein based on the nonlinear function presented in [114] for a step-type reference trajectory:

$$\psi_i = \beta_i \frac{\exp\left(-\bar{k}_i \tilde{e}_i\right) + \exp\left(\bar{k}_i \tilde{e}_i\right)}{2},$$
$$\tilde{e}_i = \begin{cases} e_i & |e_i| \le e_{max_i} \\ e_{max_i} \operatorname{sign}(e_i) & |e_i| > e_{max_i} \end{cases}, \tag{3.8}$$

where β_i, $\bar{k}_i$, and e_{max_i} are the positive tuning parameters defined by the user. β_i and $\bar{k}_i$ determine the final damping ratio and the variation rate of the nonlinear function ψ_i, respectively. The magnitude of ψ_i becomes small if the system output is far from the desired value. This provides a low damping ratio and speeds up the system response. On the sliding surface, $\bar{s} = 0$,

$$\dot{e} = -Ae, \tag{3.9}$$

where A is not a constant matrix. The following Lyapunov function was considered to verify the stability of the sliding surface $\dot{\bar{s}} = 0$:

$$V = \frac{1}{2} e^T e. \tag{3.10}$$

Substituting (3.9) into the time derivative of V leads to:

$$\dot{V} = -e^T A e. \tag{3.11}$$

A is a positive definite matrix; hence, the asymptotic stability is guaranteed.

The control law was designed, such that from any initial condition, the reference model trajectory is attracted toward the sliding surface. The following control law was designed

based on the proposed sliding surface and the feed drive dynamics:

$$\begin{aligned} \bar{u} &= J_e\left(\ddot{x}_r + A\dot{e} + \hat{K}\bar{s} + Be\right) + B_e\dot{x} + L\text{sign}\left(\dot{x}\right), \\ B &= \text{diag}\left(\dot{\psi}_i\gamma_i\right), \quad \hat{K} = \text{diag}\left(\hat{k}_i\right), \end{aligned} \tag{3.12}$$

where $\hat{k}_i$ is the adaptive gain. Only the typical friction compensation was considered herein because of the difficulty in identification and adaption and the uncertainty dynamics compensation of the other small disturbances. The adaptive law was chosen based on the idea in [87]:

$$\dot{\hat{k}}_i = \begin{cases} \xi_i|\bar{s}_i|\text{sign}(|\bar{s}_i| - \varepsilon_i) & \text{if } \hat{k}_i > \zeta_i \\ \zeta_i & \text{otherwise} \end{cases}, \tag{3.13}$$

where ε_i, ζ_i, and ξ_i are positive constants. Parameter ζ_i is introduced to obtain positive values for $\hat{k}_i$. After the sliding mode with respect to $\bar{s}_i$ was established, the gain adaption law (3.13) allowed the gain $\hat{k}_i$ to decrease while $|\bar{s}_i| < \varepsilon_i$. In other words, gain $\hat{k}_i$ will remain at the smallest level while satisfying the required accuracy of $\bar{s}_i$.

3.3.2 Uncertainty Compensation

The real system can be different from the approximated reference model; therefore, a controller was designed to compensate for the resulting uncertainty, which was eventually defined as the difference between the real system and the referred model. The uncertainty

states are defined as follows:

$$\begin{bmatrix} z_i \\ \dot{z}_i \end{bmatrix} = \begin{bmatrix} x_i \\ \dot{x}_i \end{bmatrix} - \begin{bmatrix} \bar{x}_i \\ \dot{\bar{x}}_i \end{bmatrix}, \tag{3.14}$$

where z_i is the measurable output of the uncertainty dynamics, and x and $\bar{x}$ are the actual positions of the real system and the reference model, respectively.
The uncertainty dynamics was assumed as a second-order nonlinear dynamics [112]

$$\ddot{z}_i = q_i(z) + v_i, \tag{3.15}$$

where v_i is the control input signal of the uncertainty dynamics, and $q_i(z)$ is the unknown time-varying dynamics of the system. $q_i(z)$ is assumed to be upper-bounded by Q_i

$$|q_i| \leq Q_i. \tag{3.16}$$

The tracking error for the uncertainty dynamics is described as follows:

$$\tilde{z}_i = z_i - z_{r_i}, \tag{3.17}$$

where $\tilde{z}_i$ is the tracking error, and z_{r_i} is the desired position of the uncertainty dynamics. The control structure aims to converge the output of the uncertainty dynamics to 0. Therefore, the desired values for the uncertainty position, velocity, and acceleration were set to 0. A linear SMC was used to cancel the uncertainties and track the desired position. The following sliding surface consisting of the uncertainty error and the uncertainty error

rate was used:

$$s_i = \alpha_i \tilde{z}_i + \dot{\tilde{z}}_i, \tag{3.18}$$

where α_i is the positive constant.

The sliding surface rate was obtained by taking the time derivative of the sliding surface in (3.18) as follows:

$$\begin{aligned} \dot{s}_i &= \alpha_i \dot{\tilde{z}}_i + \ddot{\tilde{z}}_i, \\ &= \alpha_i \dot{\tilde{z}}_i + \ddot{z}_i - \ddot{\tilde{z}}_{r_i}, \\ &= q_i(z) + v_i - \ddot{z}_{r_i} + \alpha_i \dot{\tilde{z}}_i. \end{aligned} \tag{3.19}$$

The following control law v_i was used to achieve $\dot{s}_i = 0$ for the stable sliding surface [112]:

$$v_i = \ddot{z}_{r_i} - \alpha_i \dot{\tilde{z}}_i - \mu_i \text{sign}(s_i) - 2\mu_i \frac{s_i}{|s_i|}. \tag{3.20}$$

Function q_i was unknown; therefore, the control law must not contain function q_i; instead, the term $\mu_i \text{sign}(s_i)$ was added to ensure that $\dot{s} = 0$. Here, μ_i was a positive adaptive gain and chosen as follows:

$$\dot{\mu}_i = \rho_i |s_i|, \tag{3.21}$$

where ρ_i is a positive constant.

Property: The control algorithm ($u_i = \bar{u}_i + v_i$) consists of the sliding mode controller based on the uncertainty dynamics and the nonlinear sliding mode controller illustrated in Fig. 3.1.

The switching function *sign* causes the chattering phenomenon in control systems; thus,

during implementation, when $|s_i| \leq \delta_i$, the $sign$ function in (3.20) is replaced by the following equation which is typical in previous works [112].

$$\text{sign}(s_i) \simeq \frac{s_i}{|s_i| + \delta_i}. \tag{3.22}$$

If function q_i is upper-bounded by Q_i as in (3.16), and the final value of the controller gain μ_i^* in (3.20) is such that $\mu_i^* > Q_i$, then z_i asymptotically converges to 0, and the sliding motion is achieved.

3.3.3 Stability Analysis

Proof: The following Lyapunov function candidate is considered:

$$V_i = \frac{1}{2}\bar{s}_i^2 + \frac{1}{2}s_i^2 + \frac{1}{2\rho_i}\left(\mu_i - \mu_i^*\right)^2. \tag{3.23}$$

The time derivative of (3.23) is given by:

$$\dot{V}_i = \bar{s}_i\dot{\bar{s}}_i + s_i\dot{s}_i + \frac{\dot{\mu}_i}{\rho_i}\left(\mu_i - \mu_i^*\right). \tag{3.24}$$

From the time derivative of (3.7) and (3.18), (3.24) becomes

$$\begin{aligned}\dot{V}_i =& \bar{s}\left(\left(\lambda_i + \psi_i\gamma_i\right)\dot{e}_i + \dot{\psi}_i\gamma_i e_i + \ddot{e}_i\right) + \frac{\dot{\mu}_i}{\rho_i}\left(\mu_i - \mu_i^*\right) \\ &+ s_i\left(q_i(z) + v_i - \ddot{z}_{r_i} + \alpha_i\dot{\bar{z}}_i\right).\end{aligned} \tag{3.25}$$

Substituting Eqs. (3.5), (3.12), (3.20), and (3.21) into (3.25) leads to:

$$\begin{aligned}\dot{V}_i &= \bar{s}_i\left(-k_i\bar{s}_i\right) + s_i\left(q_i - \mu_i \text{sign}\left(s_i\right)\right) + |s_i|\left(\mu_i - \mu_i^*\right), \\ &= \bar{s}_i\left(-k_i\bar{s}_i\right) + |s_i|\left(Q_i - \mu_i\right) + |s_i|\left(\mu_i - \mu_i^*\right), \\ &= \bar{s}_i\left(-k_i\bar{s}_i\right) + |s_i|\left(Q_i - \mu_i^*\right).\end{aligned} \tag{3.26}$$

If the final value of the controller gain μ_i^* in (3.20) is large enough (i.e., $\mu_i^* > Q_i$), then we have a stable overall system (i.e., $\dot{V}_i < 0$), and the system stability is guaranteed.

3.4 Energy Consumption

The method proposed in [57] was used herein to calculate the energy consumption of the feed drive system. The output power P_i of a three-phase AC motor is given by:

$$P_i = \sqrt{3} P_{f_i} V_i\left(t\right) I_i\left(t\right), \tag{3.27}$$

where $V_i\left(t\right)$ and $I_i\left(t\right)$ are the instantaneous effective current and voltage of a motor, respectively, and P_{f_i} is the power factor for the i^{th} axis and can be assumed constant when the load range of the motor is greater than a certain value. From (3.27), the energy consumption is given by:

$$E_i = \sqrt{3} P_{f_i} \int_0^T V_i\left(t\right) \cdot I_i\left(t\right) dt. \tag{3.28}$$

$$I_i\left(t\right) = \frac{1}{K_{\mu_i}}\left[L_i \text{sign}(\dot{x}_i) + B_{e_i}\dot{x}_i\left(t\right) + J_{e_i}\ddot{x}_i\left(t\right)\right]. \tag{3.29}$$

$$V_i\left(t\right) = I_i\left(t\right) Z_i + K_{E_i}\dot{x}_i\left(t\right), \tag{3.30}$$

where Z_i is the motor impedance and K_{E_i} the back-EMF coefficient. (3.28)-(3.30) lead to:

$$E_i = \sqrt{3} P_{f_i} \int C_{1_i} \ddot{x}_i^2 + C_{2_i} \dot{x}_i^2 + C_{3_i} \dot{x}_i \text{sign}(\dot{x}_i) + C_{4_i} + C_{5_i} \ddot{x}_i \text{sign}(\dot{x}_i) + C_{6_i} \ddot{x}_i \dot{x}_i \, dt, \tag{3.31}$$

where

$$C_{1_i} = J_{e_i}^2 \frac{Z_i}{K_{\mu_i}^2}, \qquad C_{2_i} = B_{e_i} \left(\frac{Z_i B_{e_i}}{K_{\mu_i}^2} + \frac{K_{E_i}}{K_{\mu_i}} \right),$$
$$C_{3_i} = L_i \left(\frac{2 Z_i B_{e_i}}{K_{\mu_i}^2} + \frac{K_{E_i}}{K_{\mu_i}} \right), \qquad C_{4_i} = L_i^2 \frac{Z_i}{K_{\mu_i}^2},$$
$$C_{5_i} = 2 L_i J_{e_i} \frac{Z_i}{K_{\mu_i}^2}, \qquad C_{6_i} = J_{e_i} \left(\frac{2 Z_i B_{e_i}}{K_{\mu_i}^2} + \frac{K_{E_i}}{K_{\mu_i}} \right).$$

(3.31) determines the energy only from the motion trajectory and the constant.

3.5 Simulation and Experiment

A simulation and an experiment were conducted based on the trajectories in Fig. 3.2 for the X_1 and X_2 axes to validate the effectiveness of the proposed method. Fig. 3.3 shows the velocity profile for both the X_1 and X_2 axes. The nonlinear second-order plant in (3.3) was considered as the real system, whereas the linear model in (3.6) was considered as the reference model. In the simulation, an external disturbance of $d = [30,\ 30]^T$ N was applied to evaluate the performance in the presence of a matched uncertainty. Tables 3.1 and 3.2 present the other plant and controller parameters, respectively. k_i in Table 3.2 is a fixed gain for SMC and an initial value for the adaptive gain $\hat{k}_i$. The same system parameters were used for both the simulation and the experiment.

A comparison with Ref. [106] was made to evaluate the performance. The method

TABLE 3.1: System parameters

Axis	J_{e_i} (Ns^2/m)	B_{e_i} (Ns/m)	L_i (N)	K_{μ_i} (N/A)	K_{E_i} (Vs/m)	Z_i (Ω)	P_{f_i}
1	88.1	467.2	45.5	124.8	140.0	10.0	0.4
2	97.9	631.0	54.8	200.2	200.0	15.00	0.5

TABLE 3.2: Controller parameters

Axis	λ (s^{-1})	k_i (s^{-1})	α (s^{-1})	γ (s^{-1})	ρ (s^{-1})	β	δ
1	510	1000	10	1.5	3	5	0.1
2	510	1000	10	1.5	3	5	0.1

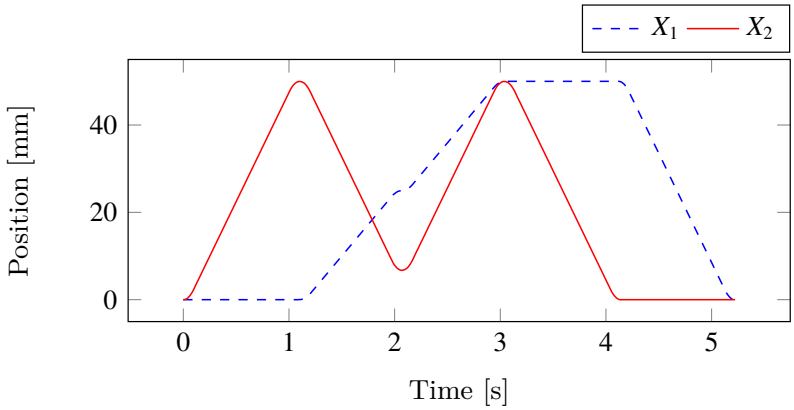

FIGURE 3.2: Reference positions

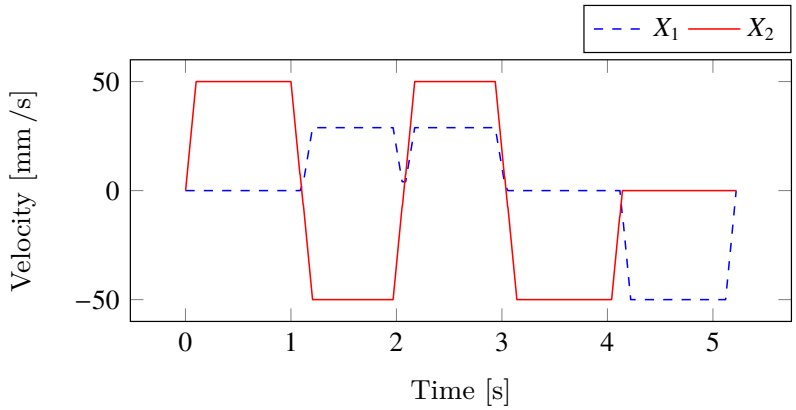

FIGURE 3.3: Reference velocities

proposed in the previous work, which is referred to as ASMC, was chosen for comparison because the sliding mode controller was robust and proven to provide a satisfactory performance under the effect of external disturbances and system uncertainties. The new method includes SMC based on the uncertainty dynamics and ASMC. The following scenarios were considered:

- adaptive SMC (ASMC) only;
- adaptive SMC with increased gain (ASMCIG);
- adaptive SMC with uncertainty dynamics (ASMCU); and
- SMC with uncertainty dynamics (SMCU).

3.5.1 Simulation Results

Fig. 3.4 shows the simulation results of the tracking performance in the X_1 and X_2 axes. With ASMC, the tracking error was larger in both axes compared to that in ASMCU and SMCU. Furthermore, the tracking performance of ASMCU was slightly better than that of SMCU. This was obvious because the adaptive part can automatically compensate for the irregular changes within the control loop. Therefore, an experimental analysis was conducted for ASMC and ASMCU only. On the contrary, Fig. 3.5 shows that the control input signals of ASMCU and SMCU were slightly larger than that of ASMC because additional control input signals were generated by the feedforward compensator in ASMCU and SMCU to compensate for the uncertainty dynamics. Table 3.3 summarizes the simulation results for clarity.

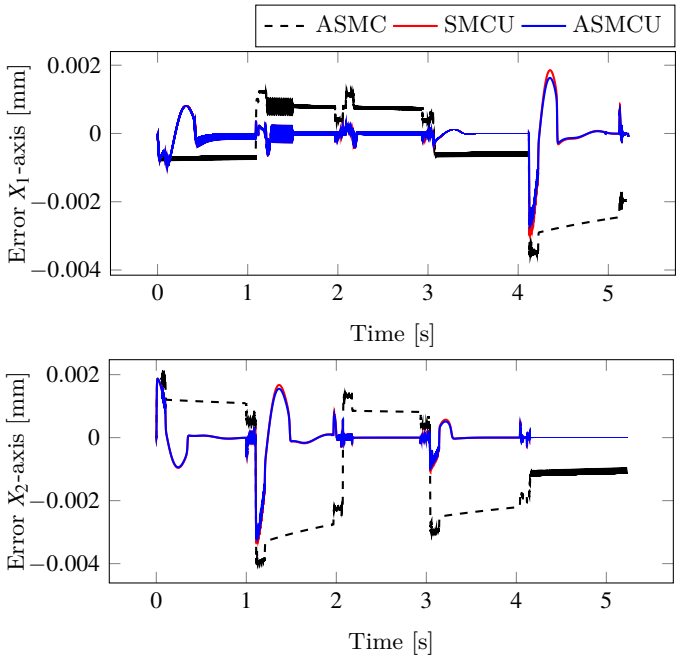

FIGURE 3.4: Simulation results of tracking error

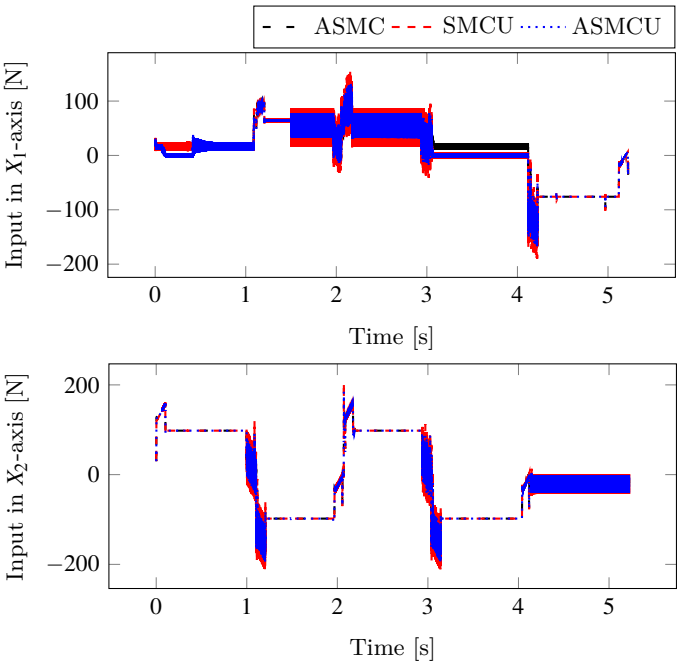

FIGURE 3.5: Simulation results of control input signal

TABLE 3.3: Summary of simulation results

Controller	Tracking error [μm]				Energy consumption [J]
	Maximum		Average		Total
	X_1-axis	X_2-axis	X_1-axis	X_2-axis	
ASMC	2.50	2.68	0.77	1.13	20.9
SMCU	1.72	2.45	0.11	0.13	21.3
ASMCU	1.65	2.44	0.11	0.13	21.3

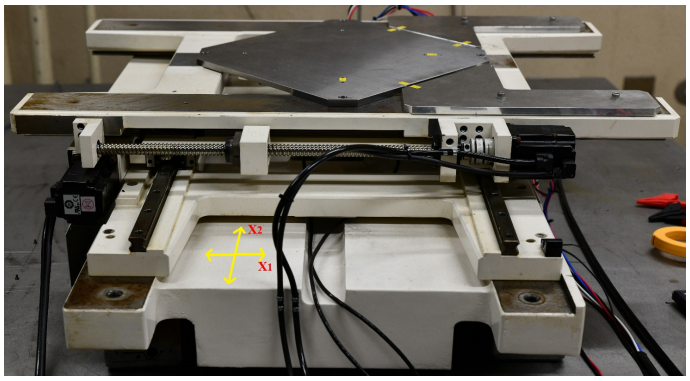

FIGURE 3.6: Industrial biaxial feed drive system

TABLE 3.4: Experimental controller parameters

Axis	λ (s^{-1})	α (s^{-1})	γ (s^{-1})	ρ (s^{-1})	β	δ
1	1200	10	1.5	2	5	0.1
2	1200	10	1.5	2	5	0.1

3.5.2 Experimental Results

An industrial biaxial ball-screw feed drive system (Fig. 3.6) was used in the experiment. The feed drive system comprised a table coupled with two ball-screw drives driven by AC servo motors connected to each drive axis. Rotary encoders (equivalent resolution: 0.076 μm) were used to measure the actual table position. The velocity signal was calculated by a numerical differentiation of the measured position. The control law was implemented using the C++ program on a personal computer with 0.2 ms sampling time.

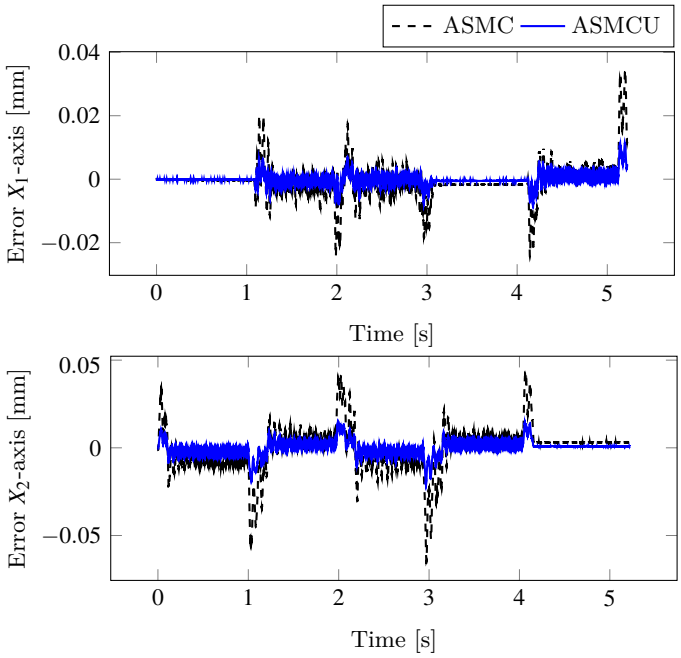

FIGURE 3.7: Experimental results of tracking error

An experiment on the trajectories was conducted in Fig. 3.2 to evaluate the tracking ability and energy-saving performance of the proposed controller. The primary aim was to confirm the effectiveness of the proposed method in the tracking performance enhancement by comparing ASMC with ASMCU. The same control parameters were applied to conduct a fare comparison (Table 3.4). Furthermore, the same initial value of the adaptive gain $\hat{k}_i$ was applied on both controllers. The electrical energy consumption was measured and analyzed by a power analyzer (HIOKI 3390). The same experiment was conducted for five times to confirm the repeatability of the proposed controller. Fig. 3.8 depicts the absolute maximum tracking errors for all the trials, where the ASMCU attained errors smaller than those in ASMC. Fig. 3.7 illustrates the tracking error results for a single trial, stating that ASMCU had a better tracking performance than ASMC. The average tracking error could be reduced by 33.33 % using ASMCU.

Fig. 3.9 shows the control input signals. The control input signal of ASMCU was slightly

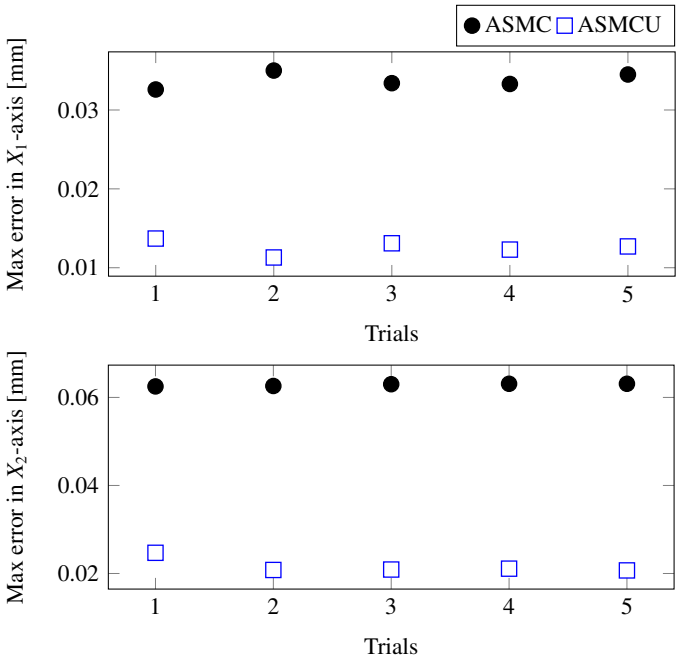

FIGURE 3.8: Experimental results of maximum tracking error

larger than that of ASMC because it generated an additional control signal to compensate for the uncertainty dynamics. The linear term λ_i of the sliding surface can be increased to allow ASMC to achieve a tracking performance similar to that of ASMCU. However, this will result in a high chattering of the input signal and lead to higher energy consumption. Furthermore, the uncertainty states converged to 0 (Fig. 3.10). Fig. 3.11 depicts the adaption of the controller gain μ_i initialized as $\mu_i(0) = 0$ for both axes. The adaption rule allowed gains to reach large final values, which stabilized the system.

TABLE 3.5: Summary of experimental results

Controller	Tracking error [mm]				Energy consumption [J]
	Maximum		Average		Total
	X_1-axis	X_2-axis	X_1-axis	X_2-axis	
ASMC	0.033	0.063	0.003	0.009	44.3
ASMCIG	0.015	0.024	0.080	0.090	45.9
ASMCU	0.013	0.021	0.001	0.007	44.9

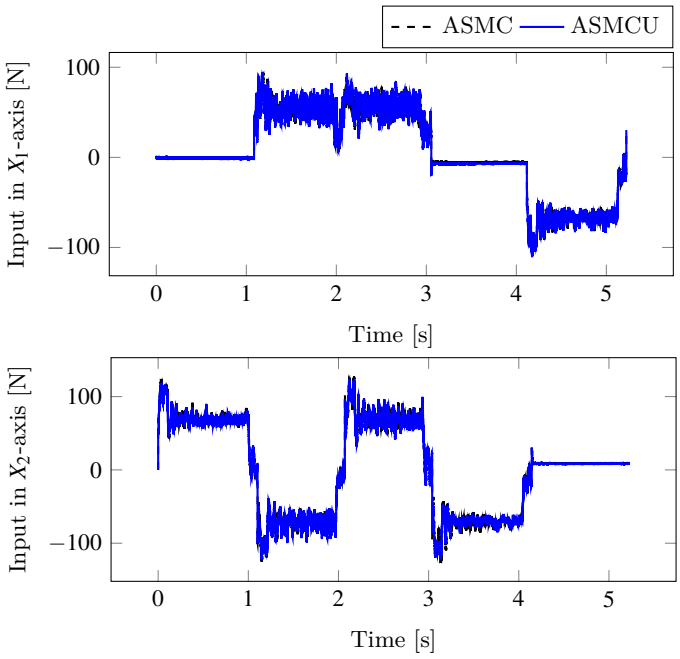

FIGURE 3.9: Control input signal

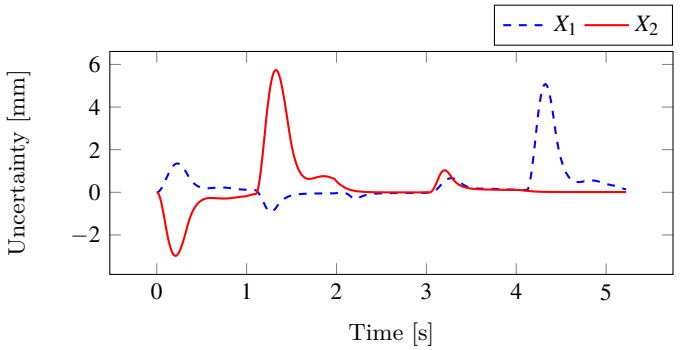

FIGURE 3.10: Uncertainty state

We then confirmed the effectiveness of the proposed method in saving energy under similar tracking performances. The linear term λ_i of the sliding surface was increased from 1200 s^{-1} to 2000 s^{-1} to achieve similar tracking performances for both ASMC and the proposed method. Fig. 3.12 shows the experimental results of the energy consumption for five trials, in which ASMCIG consumed more energy compared to ASMC and ASMCU in all trials. To achieve a good tracking performance without a compensator, disturbances

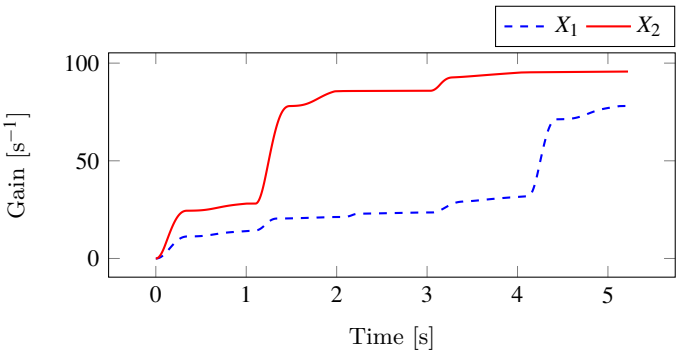

FIGURE 3.11: Controller gain μ

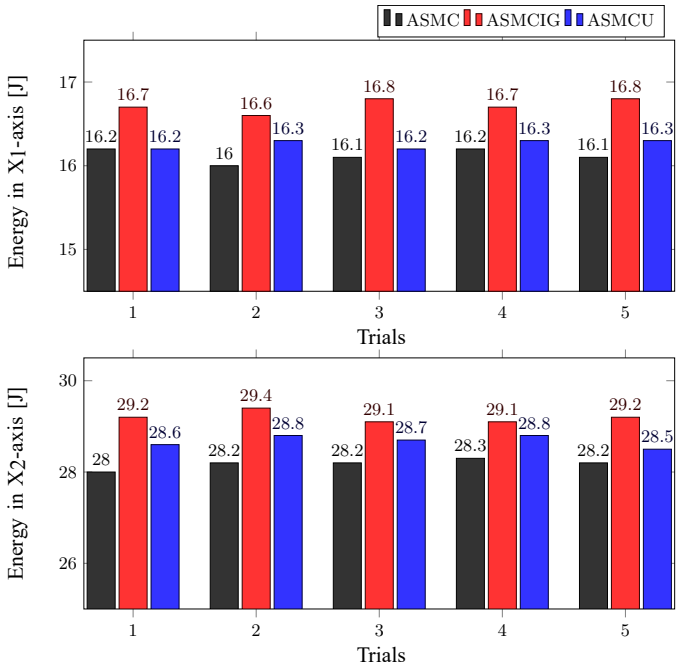

FIGURE 3.12: Energy consumption

were handled by applying high gains in the controller that increased the control input variance caused by the noise causing a higher energy consumption. On the contrary, when a compensator was used, high gains were found to be unnecessary in the controller because the disturbances were handled by the compensator, leading to less energy consumption. With the increased linear-term gain, the total energy consumed by ASMCIG increased from 44.3 J to 45.9 J on average (Table 3.5). Fig. 3.13 exhibits the tracking performance

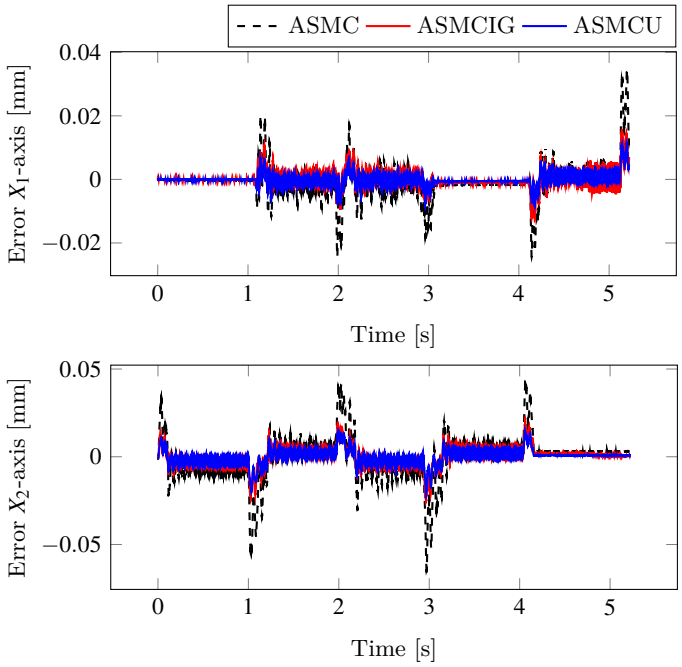

FIGURE 3.13: Experimental results of tracking error under similar tracking performance

for three cases; case 1 for the same parameters; case 2 with the increased λ_i (ASMCIG); and case 3 for ASMCU. Fig. 3.14 shows the corresponding input signals, where the control input for ASMCIG displayed more chattering compared to the others. The control input standard deviation for ASMCIG increased from 55.00 to 62.97 N compared with ASMC. The proposed method achieved an input standard deviation of 55.03 V.

3.6 Discussion

Fig. 3.15 presents the simulation results of the tracking performance in the X_1 and X_2 axes when the parameters changed. We changed the J_e and B_e values by 10 % and checked the tracking performance of the proposed controller. The obtained results, conclude that the proposed controller can still achieve a good performance. Fig. 3.16 shows the simulation results of the tracking performance in the X_1 and X_2 axes when considering

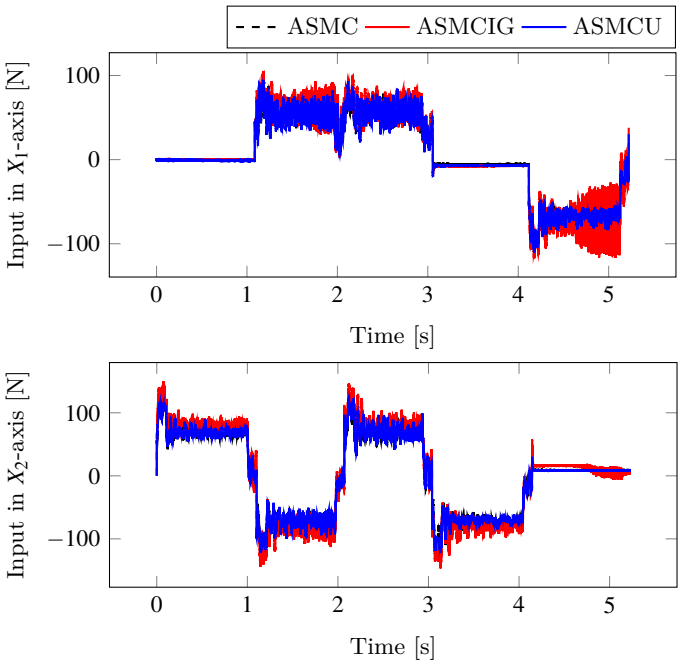

FIGURE 3.14: Control input signal under similar tracking performance

a high speed of 200 mm/s. The tracking error obtained using ASMC was larger in both axes compared to that using ASMCU. Using ASMCU could reduce the average tracking error by 67.9 %. Meanwhile, the absolute maximum tracking error could be reduced by 35.5 %. In summary, the proposed controller can be used to increase the tracking performance of high-speed feed drive systems. As a future work, it is interesting to consider including the LuGre friction model in the compensation strategy and improving contouring performance.

3.7 Conclusion

This study proposed an adaptive sliding mode control with a nonlinear sliding surface and a model-based feedforward compensator for uncertainty dynamics for application in feed drive systems. Its effectiveness was evaluated by both simulation and experimental analyses. The experimental results revealed that compared to the adaptive sliding

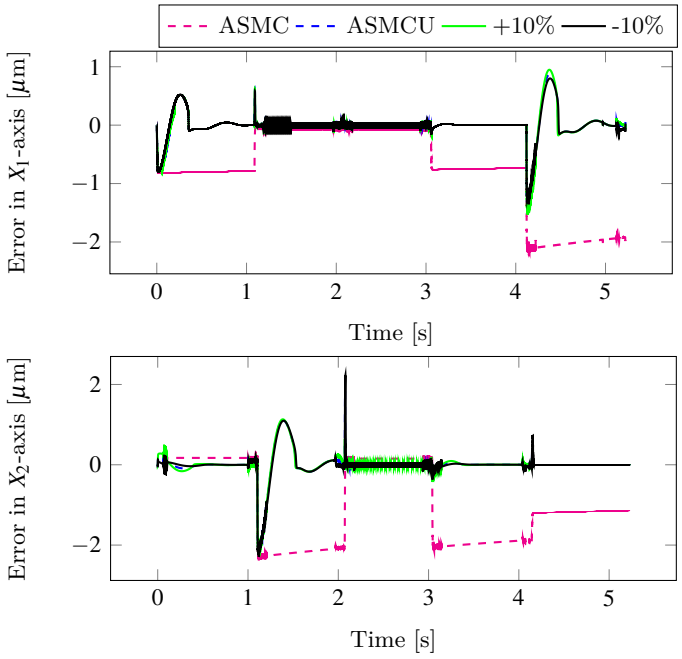

FIGURE 3.15: Simulation results under changing parameters (J_e and B_e are changed by 10 %)

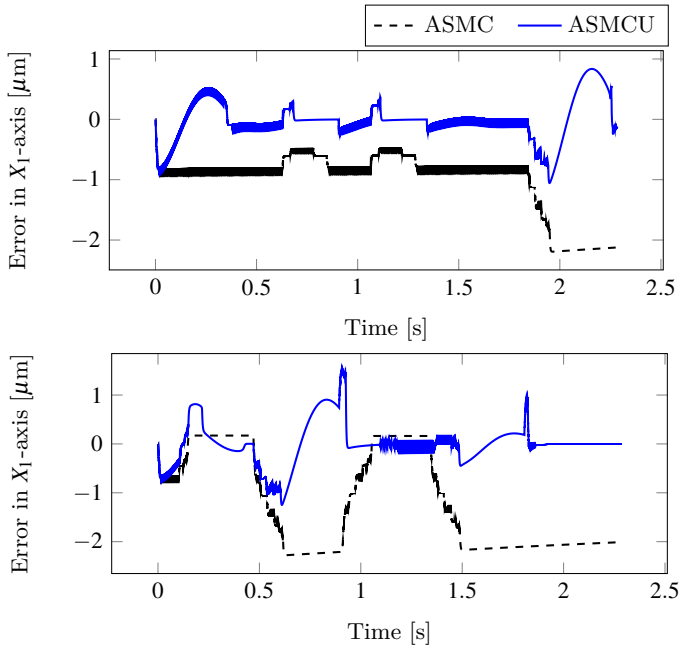

FIGURE 3.16: Simulation results under high speed (200mm/s)

mode controller, the proposed controller could achieve a substantial tracking performance, wherein the average tracking error could be reduced by 33.33 %, and the maximum tracking error could be decreased by approximately 64 % on average. In addition, the energy consumption could be reduced by 2 % on average under a similar tracking performance. A typical biaxial feed drive system was considered herein; thus, the authors believe that the proposed controller can be applied to any feed drive system configuration.

Chapter 4

Adaptive Sliding Mode Contouring Control Design based on Reference Adjustment and Uncertainty Compensation for Feed Drive Systems

4.1 Introduction

Feed drive systems are among the most dominating motion components in the production and manufacturing industries because of their wide range of use (e.g., in multi-axis motions) [88–92]. The growing demand for precise products poses the need for high-speed production systems with a higher accuracy. In addition, feed drive systems operate around the clock; therefore, they are among the major consumers of the industrial energy supply. While high-speed motion is preferred, it causes vibration in light systems, high-energy consumption, and a poor tracking performance. As explained in [74], [93], and [90], the control performance greatly depends on the system vibration, unmodeled uncertainties, and external disturbances in practical applications.

In machining, two main control approaches are used to enhance precision: tracking control approach and contouring control approach. Although many approaches for reducing the tracking errors in feed drive systems have been developed to date [8, 75, 115, 116], the most significant factor is the overall system accuracy or the system contour error [117] [3]. Contouring control is a controller design that considers the error components orthogonal to the desired contour curves, called "contour errors," as feedback signals.

A variety of alternative approaches has been developed to reduce the contour error. By calculating the contour error from the tracking errors in biaxial contour-following tasks, the authors in [118] proposed the CCC, while those in [13] decomposed the contour error into the normal tracking and advancing tangential errors. Dynamic decoupling was then applied to the system dynamics. In [119], the contour error was estimated as the vector from the actual position to the tangential line at the reference position. The authors in [120] proposed a contour-tracking controller based on polar coordinates. When using CCC methods, one of the advantages is that both the contour and tracking errors along the feed drive axes are used to calculate the control input, which causes a degradation in the contour-tracking performance.

Robust controllers, such as the sliding mode controller (SMC), provide a reasonable performance under the effect of external disturbance and system uncertainties [55, 70–74, 104]. Apart from its simplicity in design, SMC is robust against perturbation and invariant to matched uncertainties. Other SMC variants include adaptive sliding mode control (ASMC) and nonlinear sliding mode control.

Meanwhile, model-based approaches, such as feedforward friction compensation, are applied to cancel out the effect of the estimated friction force. However, friction sources generally consist of complex nonlinear properties; hence, finding an exact model is difficult, and the performance exclusively depends on the veracity of the estimated model [107] [108].

This study focused on adaptive sliding mode contouring control (ASMCC) for feed drive systems, whose main objective was to enhance the contouring performance by explicitly considering reference adjustment with addition of an uncertainty dynamics compensator. Nonlinear SMC and an additional control input were designed to compensate for the uncertainty dynamics. Accordingly, this was done by modeling the assumed uncertainty dynamics. Its controller was designed by taking the difference between a reference model and the real system based on the idea presented in [112]. The proposed method was found to enhance both the tracking and contouring performances of feed drive systems while maintaining the required energy. The system stability was analyzed and confirmed through the Lyapunov theory. In addition its convergence to the sliding surface was assured.

4.2 Controller Design

4.2.1 Contour Error Estimation

The proposed control structure comprised of a reference plant model, a real plant, and an uncertainty compensator (Fig. 4.1). This subsection explains the contouring control with a typical biaxial setup (i.e., X-Y table system), assuming the following dynamics:

$$u = M\ddot{q} + C\dot{q} + L\text{sign}(\dot{q}) + d, \tag{4.1}$$

where $q = [x,\ y]^T$, $M = \text{diag}\left(m_x,\ m_y\right)$, $C = \text{diag}\left(c_x,\ c_y\right)$, $L = \text{diag}\left(l_x,\ l_y\right)$, $d = \left[d_x, d_y\right]^T$, and $u = \left[u_x, u_y\right]^T$ are the position of the feed drive system, mass matrix, viscous coefficient matrix, Coulomb friction matrix, disturbance vector, and control input vector consisting of each axial element, respectively. The following linear equation is considered as the

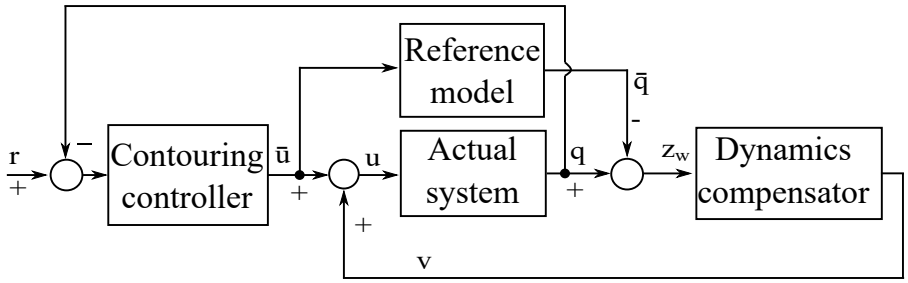

FIGURE 4.1: Block diagram of the proposed control system

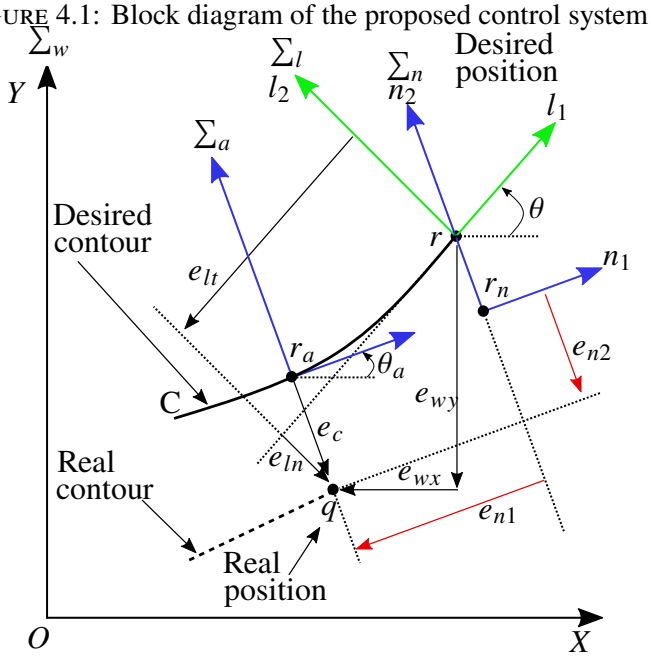

FIGURE 4.2: Definitions of tracking errors

reference model:

$$\bar{u} = M\ddot{\bar{q}} + C\dot{\bar{q}}, \tag{4.2}$$

where $\bar{q} = [\bar{q}_x,\ \bar{q}_y]^T$ and $\bar{u} = [\bar{u}_x,\ \bar{u}_y]^T$ are the position of the reference plant model and the input vector, respectively. The control input to the real plant is defined as $u = \bar{u} + v$, where $v = [v_x,\ v_y]^T$ is the compensator for the uncertainty dynamics. In machining, the tracking error reduction for each feed drive axis is not as necessary as reducing the contour error [121]. The contour error is more important because it is directly related to the shape

of the machined part in the machining application. Therefore, the proposed contouring control has a degree of freedom (DOF) tangent to the contour curve, and this DOF can be exploited for energy saving.

Fig. 4.2 schematically explains the relationship between the tracking error on each axis and the contour error. The coordinate frame $\sum_w$ is a fixed frame with x and y axes corresponding to the feed drive axes. Curve C represents the desired contour curve of the point of a feed drive. $r = \left[r_x, r_y\right]^T$ is the desired position vector of the point of the feed drive at time t defined in the coordinate frame $\sum_w$. The second derivative is required in the controller design; thus, the reference trajectory r is assumed to have C^2 continuity. Like the reference trajectory r, the real position of the feed drive q is also defined in $\sum_w$. The tracking error vector e_w of the system is given as follows:

$$e_w = [e_{wx},\ e_{wy}]^T = q - r. \tag{4.3}$$

Feed drives are generally controlled to minimize the magnitude of the tracking errors by independently controlling the drive axes. The contour error e_c is defined as the shortest distance between q and r_a. This distance is the shortest distance from q to the desired curve C. In machining, the contour error e_c, rather than the tracking error e_w, should be minimized because e_c is directly related to the shape of the machined part. In other words, if e_c is minimized to zero, the desired shape of the machined part can be realized, even though the tracking error e_w remains. The following error coordinate transformation is typical in contouring control [56]:

$$e_l = [e_{lt},\ e_{ln}]^T = R^T e_w,\ R = \begin{bmatrix} \cos\theta & -\sin\theta \\ \sin\theta & \cos\theta \end{bmatrix}, \tag{4.4}$$

where θ is the inclination of $\sum_l$ to $\sum_w$ (Fig. 4.2), and e_{lt} and e_{ln} are the tangential and normal error components to the desired contour curve at position r, respectively.

The time t_d to pass from r to r_a is approximated as follows:

$$t_d = -e_{lt} / \sqrt{\dot{r}_x^2 + \dot{r}_y^2}. \tag{4.5}$$

The estimation of r_a and the inclination θ_a of frame $\sum_a$ in Fig. 4.2 are presented as follows [56]:

$$\hat{r}_a = r(t - t_d), \hat{\theta}_a = \theta(t - t_d), \tag{4.6}$$

where $\hat{r}_a$ and $\hat{\theta}_a$ are the estimates of r_a and θ_a, respectively. $r()$ and $\theta()$ denote the functions of time:

$$\begin{aligned} r_n &= r + Q(\hat{r}_a - r), \\ Q &= \hat{R}_a S \hat{R}_a^T, S = \begin{bmatrix} 0 & 0 \\ 0 & 1 \end{bmatrix}, \end{aligned} \tag{4.7}$$

where $\hat{R}_a$ is an approximation of a rotation matrix at $\sum_a$. Matrix $\hat{R}_a$ was obtained by replacing angle θ in R in (4.4) with $\hat{\theta}_a$. The derivatives of r_n are presented below:

$$\begin{aligned} \dot{r}_n &= \dot{r} + \dot{Q}(\hat{r}_a - r) + Q(\dot{\hat{r}}_a - \dot{r}), \\ \ddot{r}_n &= \ddot{r} + \ddot{Q}(\hat{r}_a - r) + 2\dot{Q}(\dot{\hat{r}}_a - \dot{r}) + Q(\ddot{\hat{r}}_a - \ddot{r}). \end{aligned} \tag{4.8}$$

By taking the time derivative of the relation $e_n = \hat{R}_a^T e_{wn}$, where $e_n = [e_{n1},\ e_{n2}]^T$, we obtain the following:

$$\begin{aligned}
\dot{e}_n &= \hat{R}_a^T \dot{e}_{wn} + \dot{\hat{R}}_a^T e_{wn}, \\
\ddot{e}_n &= \hat{R}_a^T \ddot{e}_{wn} + 2\dot{\hat{R}}_a^T \dot{e}_{wn} + \ddot{\hat{R}}_a^T e_{wn}, \\
&= \hat{R}_a^T (\ddot{e}_{wn} + \ddot{\hat{\theta}}_a I_e e_{wn} - \dot{\hat{\theta}}_a^2 I e_{wn} + 2\dot{\hat{\theta}}_a I_e \dot{e}_{wn}), \qquad (4.9) \\
I_e &= \begin{bmatrix} 0 & 1 \\ -1 & 0 \end{bmatrix},
\end{aligned}$$

where I is a 2×2 identity matrix, and the properties of rotation matrix $\hat{R}_a \ddot{\hat{R}}_a^T = \ddot{\hat{\theta}}_a I_e - \dot{\hat{\theta}}_a^2 I$ and $\hat{R}_a \dot{\hat{R}}_a^T = \dot{\hat{\theta}}_a I_e$ are applied.

4.2.2 Adaptive Sliding Mode Contouring Controller Design

Two steps are normally involved when designing a sliding mode controller. We first considered the selection of a nonlinear sliding surface, in which the system tracks a reference trajectory. The sliding surface should ensure that the control system dynamics is exponentially stable, such that a control law that drives the system to track the desired trajectory in finite time can be designed.

The dynamic system response depends on its damping ratio [37]. Preferably, one must have a system that responds as fast as possible without overshoots. Accordingly, a variable damping ratio is applied. At the initial stage, a low damping ratio is applied to achieve a fast response. This ratio is then gradually increased to minimize overshoots. The advantage of using the variable damping ratio is that it provides a better tracking performance while reducing the energy consumption. The following nonlinear sliding surface is considered

herein [76]:

$$\bar{s} = \begin{bmatrix} A & I \end{bmatrix} \begin{bmatrix} e_n \\ \dot{e}_n \end{bmatrix},$$
$$A = \text{diag}(\lambda_j + \psi_j \gamma_j), j = \{1,\ 2\}, \tag{4.10}$$

where $\bar{s} = [\bar{s}_1,\ \bar{s}_2]^T$ is the nonlinear sliding variable vector, and λ_j is the linear term of the sliding surface. The linear term is selected by ensuring that predominant poles have a small damping ratio. γ_j is a positive linear term used to adjust the damping ratio. ψ_j is a non-negative differentiable nonlinear function of the contour error, which is upper bounded, such that $\psi_j \leq \psi_{max_j}$. Its role is to change the damping ratio of the system. Accordingly, ψ_j gradually increased the damping ratio as the contour error decreased. The following function was considerd herein based on the nonlinear function presented in [114] for a step-type reference trajectory:

$$\psi_j = \beta_j \frac{\exp\left(-\bar{k}_j \tilde{e}_{nj}\right) + \exp\left(\bar{k}_j \tilde{e}_{nj}\right)}{2},$$
$$\tilde{e}_{nj} = \begin{cases} e_{nj} & |e_{nj}| \leq e_{n_{maxj}} \\ e_{n_{maxj}} \text{sign}\left(e_{nj}\right) & |e_{nj}| > e_{n_{maxj}} \end{cases}, \tag{4.11}$$

where β_j, $\bar{k}_j$, and $e_{n_{maxj}}$ are the positive tuning parameters defined by the controller designer, and β_j and $\bar{k}_j$ determine the final damping ratio and the variation rate of the nonlinear function ψ_j, respectively. The magnitude of ψ_j becomes small if the system output is far from the desired value. This provides a low damping ratio and speeds up the system response. On the sliding surface, $\bar{s} = 0$,

$$\dot{e}_n = -A e_n, \tag{4.12}$$

where A was not a constant matrix. The following Lyapunov function was considered to verify the stability of the sliding surface, $\dot{\bar{s}} = 0$:

$$V = \frac{1}{2} e_n^T e_n. \tag{4.13}$$

Substituting (4.12) into the time derivative of V leads to:

$$\dot{V} = -e_n^T A e_n. \tag{4.14}$$

A is a positive definite matrix; thus, the asymptotic stability is guaranteed. The control law is designed such that from any initial condition, the reference model trajectory is attracted toward the sliding surface. The following control law is designed based on the proposed sliding surface and the feed drive dynamics:

$$\begin{aligned} \bar{u} =& M \left\{ \ddot{r}_n - \hat{R}_a \left(A\dot{e}_n + Be_n + \hat{K}\bar{s} \right) \right. \\ & \left. -\ddot{\hat{\theta}}_a I_e e_{wn} + \dot{\hat{\theta}}_a^2 I e_{wn} - 2\dot{\hat{\theta}}_a I_e \dot{e}_{wn} \right\} + C\dot{q} + L\,\mathrm{sign}\left(\dot{q}\right), \\ & B = \mathrm{diag}\left(\dot{\psi}_j \gamma_j\right), \quad \hat{K} = \mathrm{diag}\left(\hat{k}_j\right), \end{aligned} \tag{4.15}$$

where L is a nominal value of Coulomb friction and $\hat{k}_j$ is the adaptive gain. Only the typical friction compensation was considered because of the difficulty in identification and the adaption and uncertainty dynamics compensation of other small disturbances. The

adaption law was chosen based on the idea presented in [87]:

$$\dot{\hat{k}}_j = \begin{cases} \xi_j |\bar{s}_j| \text{sign}(|\bar{s}_j| - \varepsilon_j) & \text{if } \hat{k}_j > \zeta_j \\ \zeta_j & \text{otherwise} \end{cases}, \tag{4.16}$$

where ε_j, ζ_j, and ξ_j are positive constants. Parameter ζ_j was introduced to obtain positive values for $\hat{k}_j$. After the sliding mode with respect to $\bar{s}_j$ was established, the gain adaption law (4.16) allowed the gain $\hat{k}_j$ to decrease while $|\bar{s}_j| < \varepsilon_j$. In other words, gain $\hat{k}_j$ will remain at the smallest level while satisfying the required accuracy of $\bar{s}_j$.

4.2.3 Uncertainty Compensation

The real plant was different from the reference plant model; therefore, a controller was designed to compensate for the resulting uncertainty, which was eventually determined as the difference between the real plant and the reference plant model. Similar to the actual position of the real plant, the reference plant model was also defined in $\sum_w$. The uncertainty states are defined as follows:

$$z_w = q - \bar{q}, \tag{4.17}$$

where $z_w = \left[z_x, z_y\right]^T$ is the measurable vector in Fig. 4.1. With respect to $\sum_n$ in Fig. 4.2, the uncertainty states are expressed as $z_n = \hat{R}_a^T z_{wn}$, where $z_n = [z_{n_1}, z_{n_2}]^T$ and $z_{wn} = z_w$ when r_n is used as the desired position. The uncertainty dynamics was assumed as a

second-order nonlinear dynamics as follows:

$$\ddot{z}_n = \sigma(z_n) + v, \tag{4.18}$$

where $v = \left[v_x,\ v_y\right]^T$ is the control input signal of the uncertainty dynamics, and $\sigma(z_n) = [\sigma_1,\ \sigma_2]^T$ is the unknown time-varying dynamics of the system. σ was assumed to be upper-bounded by σ_{max} as:

$$|\sigma_j| \leq \sigma_{jmax}. \tag{4.19}$$

The tracking error for the uncertainty dynamics is defined as follows:

$$\tilde{z}_{wn} = z_{wn} - z_{rwn},\ \ \tilde{z}_n = \hat{R}_a^T \tilde{z}_{wn}, \tag{4.20}$$

where $\tilde{z}_{wn} = [\tilde{z}_{wn_1},\ \tilde{z}_{wn_2}]^T$ and $\tilde{z}_n = [\tilde{z}_{n_1},\ \tilde{z}_{n_2}]^T$ are the tracking error vectors in the $\sum_w$ and $\sum_n$ coordinate frames, respectively, and $z_{rwn} = [z_{rwn_1},\ z_{rwn_2}]^T$ is the desired position vector of the uncertainty dynamics. The control objective was to converge the output of the uncertainty dynamics to zero; thus, the desired value for the uncertainty position, velocity, and acceleration were set to 0.

A linear SMC was used to cancel out the uncertainties. The following sliding surface $s = [s_1,\ s_2]^T$ consisting of the uncertainty error and the uncertainty error rate was used as:

$$s = \alpha \tilde{z}_n + \dot{\tilde{z}}_n, \tag{4.21}$$

where $\alpha = \text{diag}\,(\alpha_1,\ \alpha_2)$ is the positive constant diagonal matrix. The sliding surface rate was obtained by taking the time derivative of the sliding surface in (4.21) as follows:

$$\begin{aligned} \dot{s} &= \alpha\dot{\tilde{z}}_n + \ddot{\tilde{z}}_n = \alpha\dot{\tilde{z}}_n + \ddot{z}_n - \ddot{z}_{r_n}, \\ &= \sigma(z) + v - \ddot{z}_{r_n} + \alpha\dot{\tilde{z}}_n, \end{aligned} \tag{4.22}$$

where $z_{rn} = \hat{R}_a^T z_{rwn}$.

Defining the Lyapunov function candidate as

$$V_s = \frac{1}{2}s^2. \tag{4.23}$$

the following function provides $s \longrightarrow 0$:

$$\begin{aligned} v &= \ddot{z}_{r_n} - \alpha\dot{\tilde{z}}_n - \mu\text{sign}\,(s)\,, \\ \mu &= \text{diag}\,(\mu_1, \mu_2)\,, \end{aligned} \tag{4.24}$$

where the positive adaptive gain μ_j is greater than σ_{jmax} in (4.19). Here μ was chosen as follows:

$$\dot{\mu}_j = \rho_j |s_j|, \tag{4.25}$$

where ρ is a positive constant.

The control law contains the *sign* function; therefore, the SMC control method endures high frequency oscillations. Several methods in the literature have been proposed to solve this problem. During the experiment, we planned to apply these methods to remove the chattering effect.

Property: Let us consider control $u = \bar{u} + v$ consisting of the sliding mode contouring

controller based on the uncertainty dynamics and the nonlinear sliding mode controller illustrated in Fig. 4.1. If the function σ is upper-bounded by σ_{max} as in (4.19), and the final value of the controller gain μ_j^* in (4.24) satisfies $\mu_j^* > \sigma_{jmax}$, then z_n asymptotically converges to zero, and the sliding motion is achieved. (Proof is straightforward and omitted.)

4.2.4 Stability Analysis

The following Lyapunov function candidate was considered:

$$V = \frac{1}{2}\bar{s}^2 + \frac{1}{2}s^2 + \frac{1}{2\rho}\left(\mu - \mu^*\right)^2. \tag{4.26}$$

The time derivative of (4.26) is given by:

$$\begin{aligned}\dot{V} &= \bar{s}\dot{\bar{s}} + s\dot{s} + \frac{\dot{\mu}}{\rho}\left(\mu - \mu^*\right), \\ &= \bar{s}\left(A\dot{e_n} + Be_n + \ddot{e_n}\right) + \frac{\dot{\mu}}{\rho}\left(\mu - \mu^*\right) + s\left(\sigma\left(z\right) + v - \ddot{z}_{rn} + \alpha\dot{\tilde{z}}_n\right).\end{aligned} \tag{4.27}$$

From (4.9) we obtain:

$$\begin{aligned}\ddot{e}_n &= \hat{R}_a^T(\ddot{e}_{wn} + \ddot{\hat{\theta}}_a I_e e_{wn} - \dot{\hat{\theta}}_a^2 I e_{wn} + 2\dot{\hat{\theta}}_a I_e \dot{e}_{wn}), \\ &= \hat{R}_a^T(\ddot{q} - \ddot{r}_n + \ddot{\hat{\theta}}_a I_e e_{wn} - \dot{\hat{\theta}}_a^2 I e_{wn} + 2\dot{\hat{\theta}}_a I_e \dot{e}_{wn}), \\ &= \hat{R}_a^T(\frac{1}{M}\left(\bar{u} - C\dot{q} - L\text{sign}(\dot{q})\right) - \ddot{r}_n + \ddot{\hat{\theta}}_a I_e e_{wn} - \dot{\hat{\theta}}_a^2 I e_{wn} + 2\dot{\hat{\theta}}_a I_e \dot{e}_{wn}).\end{aligned} \tag{4.28}$$

Substituting (4.15) into (4.28) leads to the following:

$$\ddot{e}_n = -(A\dot{e}_n + Be_n + \hat{K}\bar{s}). \tag{4.29}$$

Substituting (4.29), (4.24), and (4.25) into (4.27) leads to:

$$\begin{aligned}\dot{V} &= \bar{s}(-\hat{K}\bar{s}) + |s|\,(\mu - \mu^*) + s(\sigma(z) - \mu \text{sign}(s)),\\ &= \bar{s}(-\hat{K}\bar{s}) + |s|\,(\sigma_{max} - \mu) + |s|\,(\mu - \mu^*),\\ &= \bar{s}(-\hat{K}\bar{s}) + |s|\,(\sigma_{max} - \mu^*).\end{aligned} \tag{4.30}$$

If the final value of the controller gain μ^* in (4.24) is large enough (i.e., $\mu^* > \sigma_{max}$), then we have:

$$\dot{V} < 0, \tag{4.31}$$

and the system stability is guaranteed.

4.3 Energy Consumption

The method proposed in [57] was used herein to calculate the energy consumption of the feed drive system. The output power P_i of a three-phase AC motor is given as follows:

$$P_i = \sqrt{3} P_{f_i} V_i(t)\, I_i(t), \tag{4.32}$$

whereby $V_i(t)$ and $I_i(t)$ are the instantaneous effective current and the voltage of a motor, respectively, and P_{f_i} is the power factor for the i^{th} axis that can be assumed constant when the load range of the motor is greater than a certain value. From (4.32), the energy

consumption is given as:

$$E_i = \sqrt{3} P_{f_i} \int_0^T V_i(t) \cdot I_i(t)\, dt, \tag{4.33}$$

$$I_i(t) = \frac{1}{K_{\mu_i}} \left[L_i \text{sign}(\dot{x}_i) + B_{e_i} \dot{x}_i(t) + J_{e_i} \ddot{x}_i(t) \right], \tag{4.34}$$

$$V_i(t) = I_i(t) Z_i + K_{E_i} \dot{x}_i(t), \tag{4.35}$$

where Z_i is the motor impedance and K_{E_i} is the back-EMF coefficient. (4.33)-(4.35) lead to:

$$\begin{aligned} E_i = & \sqrt{3} P_{f_i} \int C_{1_i} \ddot{x}_i^2 + C_{2_i} \dot{x}_i^2 + C_{3_i} \dot{x}_i \text{sign}(\dot{x}_i) + C_{4_i} \\ & + C_{5_i} \ddot{x}_i \text{sign}(\dot{x}_i) + C_{6_i} \ddot{x}_i \dot{x}_i \, dt, \end{aligned} \tag{4.36}$$

where

$$C_{1_i} = J_{e_i}^2 \frac{Z_i}{K_{\mu_i}^2}, \qquad C_{2_i} = B_{e_i} \left(\frac{Z_i B_{e_i}}{K_{\mu_i}^2} + \frac{K_{E_i}}{K_{\mu_i}} \right),$$

$$C_{3_i} = L_i \left(\frac{2 Z_i B_{e_i}}{K_{\mu_i}^2} + \frac{K_{E_i}}{K_{\mu_i}} \right), \qquad C_{4_i} = L_i^2 \frac{Z_i}{K_{\mu_i}^2},$$

$$C_{5_i} = 2 L_i J_{e_i} \frac{Z_i}{K_{\mu_i}^2}, \qquad C_{6_i} = J_{e_i} \left(\frac{2 Z_i B_{e_i}}{K_{\mu_i}^2} + \frac{K_{E_i}}{K_{\mu_i}} \right).$$

(4.36) determines the energy only from the motion trajectory and the constant.

4.4 Simulation

A simulation was conducted based on a reference trajectory in (4.37) and Fig. 4.3 for the x and y axes to validate the effectiveness of the proposed method, .

$$\begin{aligned} x_r &= r\cos(\frac{2\pi t}{T}), \\ y_r &= r\sin(\frac{2\pi t}{T}), \end{aligned} \tag{4.37}$$

where r is the radius, and T is the total time taken to complete the trajectory. Tables 4.1 and 4.2 present the plant and controller parameters, respectively. A comparison with the results in [75], was made to evaluate the performance. The proposed method includes contouring ASMC with reference adjustment and SMC based on uncertainty dynamics. The following scenarios were considered:

- ASMC only for tracking in each drive axis (Track);
- ASMC for contouring control with reference adjustment (CC); and
- ASMCC and uncertainty dynamics (CCU).

The nonlinear second-order plant in (4.1) was considered as the real plant, whereas the linear model in (4.2) was considered as the reference plant model. The Coulomb friction

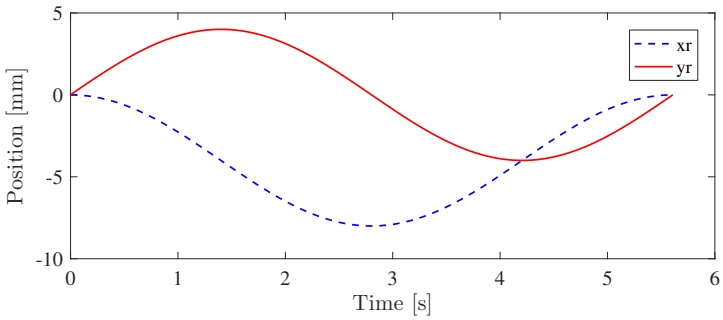

FIGURE 4.3: Reference trajectories

force L in the real plant (4.1) was set to vary with time as in (4.38) to evaluate the performance in presence of a matched uncertainty. An array of random numbers, whose elements were normally distributed with mean 0, variance, and standard deviation, was added as an external disturbance vector, d.

$$L\text{sign}(\dot{q}) = \begin{cases} L\text{sign}(\dot{q}) & \text{if } 0\,\text{s} \leq t < 1.6\,\text{s} \\ 0 & \text{if } 1.6\,\text{s} \leq t < 3\,\text{s} \\ 0.5L\text{sign}(\dot{q}) & \text{if } 3\,\text{s} \leq t < 4.4\,\text{s} \\ 1.5L\text{sign}(\dot{q}) & \text{if } 4.4\,\text{s} \leq t \leq 5.6\,\text{s} \end{cases} \tag{4.38}$$

4.4.1 Simulation Results

Simulation Results Under Low Speed

We first evaluated the performance of the proposed approach under a low speed of 4.5 [mm/s]. Fig. 4.4 depicts the tracking performance results in the x and y axes. With the Track, the average tracking error was larger in both axes compared to that of CC and CCU. Fig. 4.5 shows the tracking error results in the $\sum_n$ coordinate frame. Both e_{n1} and e_{n2} were larger with the Track compared to that of CC and CCU. Accordingly, e_{n2}, which was used as an estimate of the contour error e_c, was minimum when CCU was applied. Fig. 4.6 illustrates the control input signals. The control input signals of the CCU were slightly larger than those of the Track and the CC only because the CCU generated an additional control signal v to compensate for the uncertainty dynamics. The linear term λ_j of the

TABLE 4.1: System parameters

Axis	M (Ns^2/m)	C (Ns/m)	L (N)
x	88.08	467.20	45.50
y	97.90	631.00	54.80

TABLE 4.2: Controller parameters

Axis	$\lambda\,(\mathrm{s}^{-1})$	$\alpha\,(\mathrm{s}^{-1})$	$\gamma\,(\mathrm{s}^{-1})$	$\rho\,(\mathrm{s}^{-1})$	β
x	200	60	1.2	0.5	6
y	200	60	1.2	0.5	6

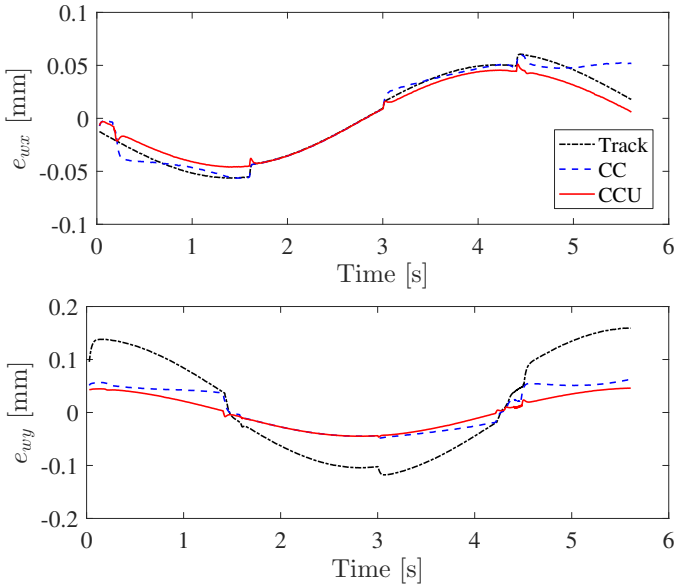

FIGURE 4.4: Tracking errors e_w

sliding surface $\bar{s}_j$ can be increased to allow the CC to achieve a contouring performance similar to that of the CCU, . However, note that this will result in a higher chattering of the input signal, which will lead to a higher energy consumption. Fig. 4.7 exhibits the adaption of the controller gain μ. The gain was initialized as $\mu_j(0) = 0$. Moreover, the gain reached a large final value because of the adaption rule, which consequently stabilized the system. Fig. 4.8 shows the result of the varied Coulomb friction force L. If we relate the findings to the results of the normal and tangential errors in Fig. 4.5, we can see that the CC has a large error when the L magnitude increases and almost the same error as the CCU when the L magnitude is zero at $1.6\,\mathrm{s} \leq t \leq 3\,\mathrm{s}$. However, CCU had almost the same magnitude of errors all throughout, independent of the changing magnitude of L, because of the addition of the uncertainty compensator that compensated for these changes. Using

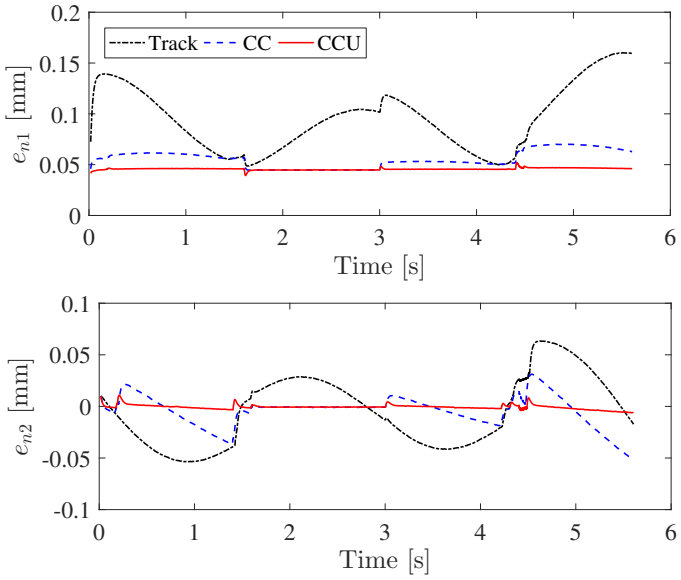

FIGURE 4.5: Tangential and normal error e_n

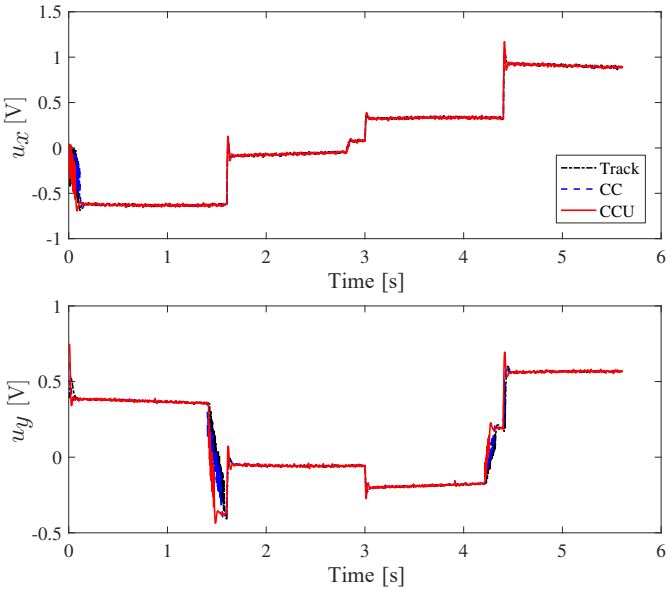

FIGURE 4.6: Control input u

CCU reduced the average contour error by 85.71 %. The absolute maximum contour error could be reduced by 78.64 % compared with CC. Table 4.3 summarizes the simulation results under low speed for clarity.

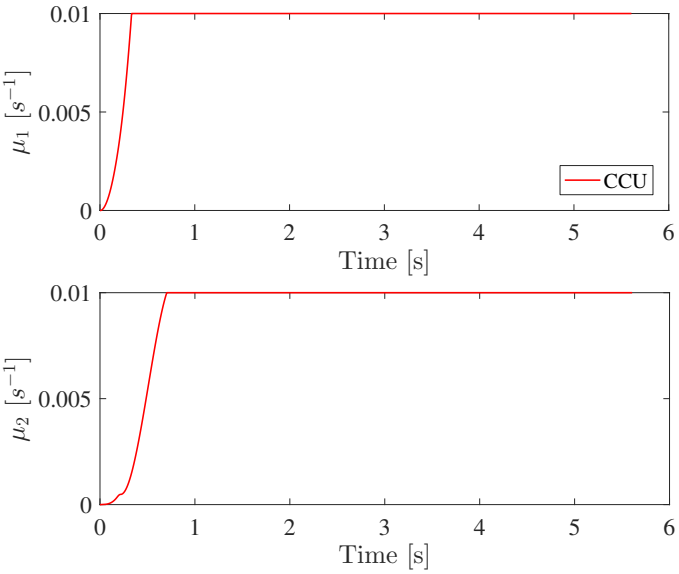

FIGURE 4.7: Controller gain μ

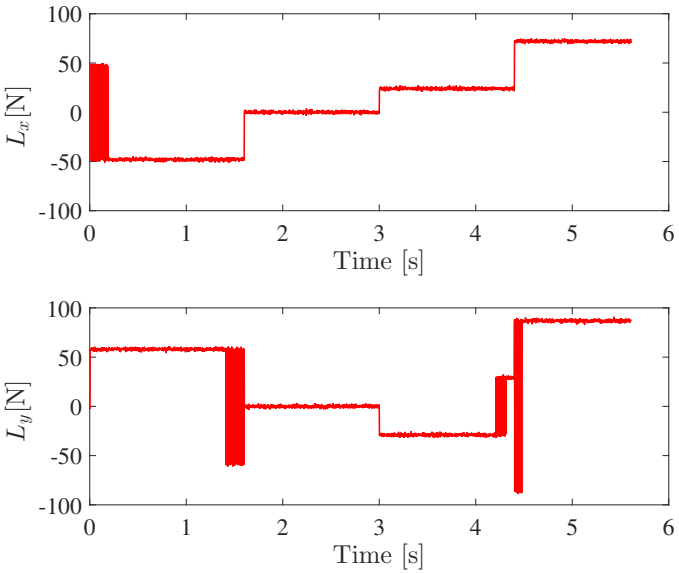

FIGURE 4.8: Coulomb friction force L

Simulation Results Under High Speed

We then evaluated the performance of the proposed approach under a high speed of 100 [mm/s]. Fig. 4.9 depicts the results of the tracking performance e_w. The tracking

TABLE 4.3: Summary of the results under low speed of 4.5 [mm/s]

Controller	Tangential and Normal error [mm]				Energy consumption [μJ]
	Maximum		Average		Total
	e_{n1}	e_{n2}	e_{n1}	e_{n2}	
ASMCT	0.1602	0.0634	0.0947	0.0306	1.3362
ASMCC	0.0701	0.0515	0.0556	0.0112	1.3281
ASMCCU	0.0521	0.0110	0.0457	0.0016	1.3568

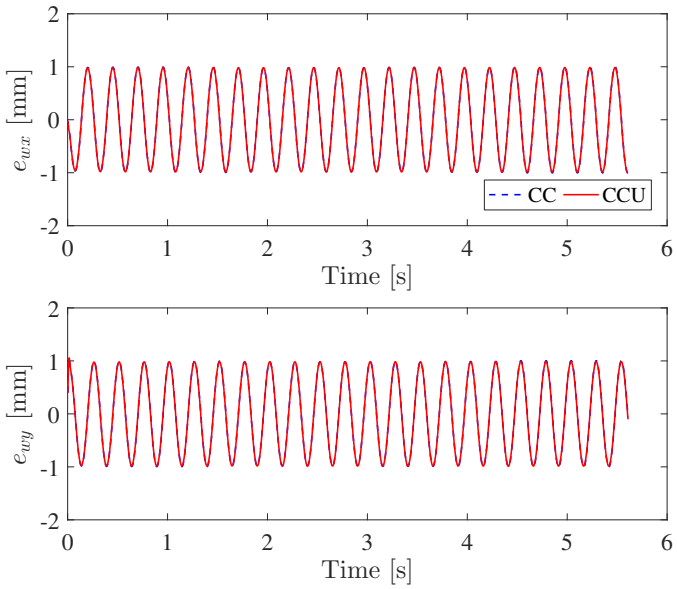

FIGURE 4.9: Tracking control e_{wx} under high speed

performances of both CC and CCU were almost the same. Fig. 4.10 shows the performance in the $\sum_n$ coordinate frame. As with the low speed, CCU achieved the smallest error in both the e_{n1} and e_{n2} directions compared to CC. The e_n results when using the tracking controller were not included in Fig. 4.10 because they were too big when high speed was used. Using CCU could reduce the average contour error by 4.48 %. Meanwhile, the absolute maximum contour error could be reduced by 10.13 % compared to CC. In conclusion, the proposed controller can be used to increase the contouring performance in high-speed feed drive systems. Table 4.4 summarizes the simulation results under high

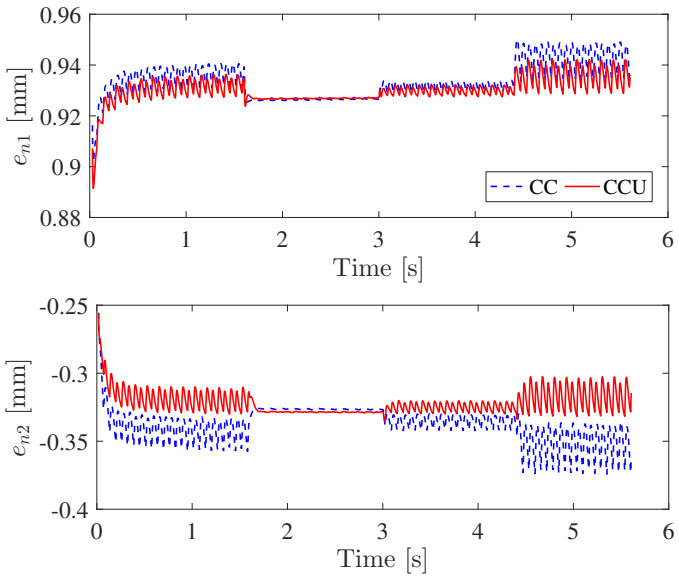

FIGURE 4.10: Tangential and normal error e_n under high speed

TABLE 4.4: Summary of the results under high speed 100 [mm/s]

Controller	Tangential and Normal error [mm]				Energy consumption [μJ]
	Maximum		Average		Total
	e_{n1}	e_{n2}	e_{n1}	e_{n2}	
ASMCT	2.0592	1.1682	1.4378	0.5577	5.8524
ASMCC	0.9553	0.3789	0.9402	0.3429	4.7804
ASMCCU	0.9486	0.3407	0.9370	0.3275	4.8848

speed for clarity.

4.5 Conclusion

This study proposed as an approach the combination of an adaptive sliding mode contouring controller with reference adjustment and sliding mode control based on uncertainty dynamics for the precision motion in a feed drive system. The feasibility of the approach

was then demonstrated by the simulation results. The proposed method showed a substantial improvement in performance by reducing the average contour error by 85.71 % and the maximum contouring error by 78.64 % under a low speed compared to the adaptive sliding mode contouring controller with reference adjustment. Under high speed, the proposed approach reduced the average and absolute maximum contour errors by 4.48 % and 10.13 %, respectively. The experimental verification is left for future work.

Chapter 5

Conclusions and Future Works

5.1 Conclusions

With regards to modern CNC machine tools, robotics, and industrial applications, the demand for fast response, high precision, and energy saving has become the priority of the machine tool control community. Over the years, the research community has invested in precision control and energy saving for these systems. This dissertation presented adaptive sliding mode control with a nonlinear sliding surface to enhance tracking performance of industrial feed drive systems and reduce their energy consumption. A feedforward compensator for plant uncertainties was also designed. Accordingly, this dissertation presented an adaptive sliding mode contouring controller based on reference adjustment and an uncertainty compensator for the biaxial feed drive system to improve the contouring performance in feed drive systems. Furthermore, simulations and experiments were conducted to examine the effectiveness of the proposed controllers.

The main contributions of this dissertation are as follows:

1. We presented an adaptive sliding mode controller with a nonlinear sliding surface for ball-screw feed drive systems to enhance the tracking performance and reduce the consumed energy of industrial feed drive systems. We verified the effectiveness of the proposed controller via simulations and experiments. Two cases were considered

herein. The first case showed the effectiveness of the proposed adaptive nonlinear sliding mode control in improving the tracking performance. The second case showed the ability of the proposed approach to reduce energy consumption and control input variance. In the first case, the average tracking error was reduced by 46.9 % without additional electrical energy or control input variation. In the second case, the proposed approach reduced both the energy consumption and the control input varience by 13.3 % and 15.2 %, respectively.

2. The proposed adaptive sliding mode controller with a nonlinear sliding surface was extended to consider the uncertainty compensation. An adaptive sliding mode controller with feedforward compensator for the precision motion of feed drive systems was presented. The effectiveness of adding the uncertainty compensator was verified through both simulation and experiments based on the pentagon trajectory. The experimental results verified that compared to the adaptive sliding mode controller, the proposed approach achieved a substantial tracking performance, wherein the average and maximum tracking errors were reduced by 33.3 % and approximately 64 % on average, respectively. We also showed the ability of the proposed approach to reduce the energy consumption. Consequently, the proposed approach could reduce the energy consumption by 2 % on average under a similar tracking performance. A typical biaxial feed drive system was used herein; thus, we believe that the proposed controller can be applied to any feed drive system configuration.

3. Finally, we proposed herein a combined approach of the adaptive sliding mode contouring controller with reference adjustment and a sliding mode controller based on the uncertainty dynamics for the precision motion of industrial feed drive systems. The controller aims to enhance the contouring performance by explicitly considering reference adjustment with the addition of the uncertainty dynamics compensator.

The effectiveness of the proposed controller with reference adjustment and the uncertainty dynamics compensator was verified through a computer simulation. As a result, the proposed approach showed a substantial improvement in performance by reducing the average contour error by 85.71 % and the maximum contouring error by 78.64 % compared to the adaptive sliding mode contouring controller without the uncertainty compensator.

5.2 Future Work

For the future research work, some suggestions for improving the contouring performance of industrial feed drive systems are listed below:

1. In this dissertation, we verified that employing an adaptive sliding mode controller results in an enhanced tracking performance compared to a nonadaptive sliding mode controller. Selecting the adaptive law is not unique, but other functions may produce even improved results. Therefore, we will consider designing optimal adaption laws based on reducing the tracking or contour error and control input variance in our future work.

2. In the proposed adaptive sliding mode control for precision enhancement of industrial feed drive systems, the traditional sign function is still utilized in the controller design to drive the system onto the sliding surface. In other words, the chattering phenomenon will exist, particularly in the feed drive systems. However, such a phenomenon and its corresponding influences should be well addressed.

3. Implementation of the proposed approach presented in Chapter 4 for the two-axis machine. The proposed contouring controller with the uncertainty compensator

improved the contouring performance. Hence, the proposed approach is expected to improve the contouring performance in multi-axes machining tasks.

Appendix A

List of Publications

Journal papers:

J.1. E. W. Nshama, M. R. Msukwa and N. Uchiyama, "Pareto optimal trajectory generation along piecewise linear paths with smoothed corners via a trade-off between energy saving and cycle time reduction in industrial feed drive systems," (Submitted).

J.2. M. R. Msukwa, E. W. Nshama and N. Uchiyama, "Adaptive Sliding Mode Control with Feedforward Compensator for Energy-Efficient and High-Speed Precision Motion of Feed Drive Systems," IEEE Access, IF: 4.64, vol. 8, pp. 43571-43581, 2020.

J.3. M. R. Msukwa and N. Uchiyama, "Design and Experimental Verification of Adaptive Sliding Mode Control for Precision Motion and Energy Saving in Feed Drive Systems," IEEE Access, IF: 4.64, vol. 7, pp. 20178-20186, 2019.

J.4. K. R. Simba, B. D. Bui, M. R. Msukwa, and N. Uchiyama, "Robust iterative learning contouring controller with disturbance observer for machine tool feed drives," ISA Transactions, IF: 5.20, vol. 75, pp. 207-215, 2018.

Conference papers:

C.1. M. R. Msukwa, E. W. Nshama and N. Uchiyama, "Contouring Control Based on Reference Adjustment and Uncertainty Compensator for Precision Motion of Industrial Feed Drive Systems," *2020 IEEE 29th International Symposium on Industrial Electronics (ISIE)*, Delft, The Netherlands, 2020, pp. 89-94.

C.2. M. R. Msukwa, E. W. Nshama and N. Uchiyama, "Adaptive Sliding Mode Control for Precision Motion of Industrial Feed Drive Systems with Uncertainty Dynamics," *2019 American Control Conference (ACC)*, Philadelphia, USA, 2019, pp. 1718-1723.

C.3. E. W. Nshama, M. R. Msukwa and N. Uchiyama, "Pareto Optimization of Energy and Tolerance in Motion Trajectory Generation for Industrial Feed Drive Systems," *2019 American Control Conference (ACC)*, Philadelphia, USA, 2019, pp. 842-847.

C.4. M. R. Msukwa, N. Uchiyama and B. Dinh Bui, "Adaptive nonlinear sliding mode control with a nonlinear sliding surface for feed drive systems." *2017 IEEE International Conference on Industrial Technology (ICIT)*, Toronto, ON, Canada, 2017, pp. 732-737.

Bibliography

[1] C. Okwudire, "Modeling and control of high speed machine tool feed drives," Ph.D. dissertation, The University of British Columbia, 2009.

[2] B. D. Bui, N. Uchiyama, and K. R. Simba, "Contouring control for three-axis machine tools based on nonlinear friction compensation for lead screws," *International Journal of Machine Tools and Manufacture*, vol. 108, pp. 95–105, 2016.

[3] R. Ramesh, M. Mannan, and A. Poo, "Tracking and contour error control in cnc servo systems," *International Journal of Machine Tools and Manufacture*, vol. 45, no. 3, pp. 301 – 326, 2005.

[4] Y. Altintas, A. Verl, C. Brecher, L. Uriarte, and G. Pritschow, "Machine tool feed drives," *CIRP Annals-Manufacturing Technology*, vol. 60, no. 2, pp. 779–796, 2011.

[5] H. Schulz and T. Würz, "Balancing requirements for fast rotating tools and spindle systems," *CIRP Annals-Manufacturing Technology*, vol. 47, no. 1, pp. 321–324, 1998.

[6] M. Tomizuka, "Zero phase error tracking algorithm for digital control," *Journal of Dynamic Systems, Measurements, and Control*, vol. 109, no. 1, pp. 65–68, 1987.

[7] G. Pritschow and W. Philipp, "Research on the efficiency of feedforward controllers in m direct drives," *CIRP Annals-Manufacturing Technology*, vol. 41, no. 1, pp. 411–415, 1992.

[8] Y. Altintas, K. Erkorkmaz, and W.-H. Zhu, "Sliding mode controller design for high speed feed drives," *CIRP Annals*, vol. 49, no. 1, pp. 265 – 270, 2000.

[9] A. Kamalzadeh and K. Erkorkmaz, "Accurate tracking controller design for high-speed drives," *International Journal of Machine Tools and Manufacture*, vol. 47, pp. 1393–1400, 2007.

[10] H. V. Brussel and P. V. den Braembussche, "Robust control of feed drives with linear motors," *CIRP Annals*, vol. 47, no. 1, pp. 325 – 328, 1998.

[11] Y. Korean, "Cross-coupled biaxial computer control for manufacturing systems," *ASME Journal of Engineering for Industry*, vol. 102, no. 4, pp. 265 – 272, 1980.

[12] Z. M. Yeh, Y. Tarng, and Y. Lin, "Cross-coupled fuzzy logic control for multiaxis machine tools," *Mechatronics*, vol. 7, no. 8, pp. 663 – 681, 1997.

[13] H. C. Ho, J. Y. Yen, and S. S. Lu, "A decoupled path-following control algorithm based upon the decomposed trajectory error," *International Journal of Machine Tools and Manufacture*, vol. 39, no. 10, pp. 1619 – 1630, 1999.

[14] G. T. Chiu and M. Tomizuka, "Contouring control of machine tool feed drive systems: a task coordinate frame approach," *IEEE Transactions on Control Systems Technology*, vol. 9, no. 1, pp. 130–139, 2001.

[15] M. Y. Cheng, K. H. Su, and S. F. Wang, "Contour error reduction for free-form contour following tasks of biaxial motion control systems," *Robotics and Computer-Integrated Manufacturing*, vol. 25, no. 2, pp. 323 – 333, 2009.

[16] K. H. Su and M. Y. Cheng, "Contouring accuracy improvement using cross-coupled control and position error compensator," *International Journal of Machine Tools and Manufacture*, vol. 48, no. 12, pp. 1444 – 1453, 2008.

[17] C. C. Lo and C. Y. Chung, "Tangential-contouring controller for biaxial motion control," in *ASME, Journal of Dynamic Systems, Measurements, and Control.*, vol. 121, 1999, pp. 126–129.

[18] M. Y. Cheng and C. C. Lee, "On real-time contour error estimation for contour following tasks," in *Proceedings, 2005 IEEE/ASME International Conference on Advanced Intelligent Mechatronics.*, 2005, pp. 1047–1052.

[19] X. Ye, X. Chen, X. Li, and S. Huang, "A cross-coupled path precompensation algorithm for rapid prototyping and manufacturing," in *The International Journal of Advanced Manufacturing Technology.*, vol. 20, 2002, pp. 39–43.

[20] Y. Tarng, H. Chuang, and W. Hsu, "Intelligent cross-coupled fuzzy feedrate controller design for cnc machine tools based on genetic algorithms," *International Journal of Machine Tools and Manufacture*, vol. 39, no. 10, pp. 1673 – 1692, 1999.

[21] J. H. Chin, Y. M. Cheng, and J. H. Lin, "Improving contour accuracy by fuzzy-logic enhanced cross-coupled precompensation method," *Robotics and Computer-Integrated Manufacturing*, vol. 20, no. 1, pp. 65 – 76, 2004.

[22] S. S. Yeh and P. L. Hsu, "Adaptive-feedrate interpolation for parametric curves with a confined chord error," *Computer-Aided Design.*, vol. 34, pp. 229–237, 2002.

[23] S. Jee and Y. Koren, "Adaptive fuzzy logic controller for feed drives of a cnc machine tool," *Journal of Mechatronics*, vol. 14, no. 3, pp. 299 – 326, 2004.

[24] U. Itkis, "Control systems of variable structure," *Wiley, New York*, 1976.

[25] V. Utkin, "Variable structure systems with sliding modes," *IEEE Transactions on Automatic Control*, vol. 22, no. 2, pp. 212–222, 1977.

[26] J. Guldner and V. I. Utkin, "Tracking the gradient of artificial potential fields: sliding mode control for mobile robots," *International Journal of Control*, vol. 63, no. 3, pp. 417–432, 1996.

[27] A. S. I. Zinober, O. M. E. Ei-Ghezawi, and S. A. Billings, "Multivariable variable-structure adaptive model-following control systems," *IEE Proceedings D - Control Theory and Applications*, vol. 129, no. 1, pp. 6–12, 1982.

[28] J. E. Slotine, J. K. Hedrick, and E. A. Misawa, "On Sliding observers for nonlinear systems," *Journal of Dynamic Systems, Measurement, and Control*, vol. 109, no. 3, pp. 245–252, 1987.

[29] S. Drakunov and V. Utkin, "Sliding mode observers: A tutorial," in *Proceedings of 1995 34th IEEE Conference on Decision and Control, New-Orleans, LA, USA*, vol. 4, 1995, pp. 3376–3378.

[30] B. Drazenovic, "The invariance conditions in variable structure systems," *Automatica*, vol. 5, no. 3, pp. 287 – 295, 1969.

[31] K. Furuta, "Sliding mode control of a discrete system," *Systems and Control Letters*, vol. 14, no. 2, pp. 145 – 152, 1990.

[32] H. Sira-Ramirez, "Differential geometric methods in variable-structure control," *International Journal of Control*, vol. 48, pp. 1359–1390, 1988.

[33] R. A. De Carlo, S. H. Zak, and G. P. Matthews, "Variable structure control of nonlinear multivariable systems: A tutorial," *Proceedings of the IEEE*, vol. 76, no. 3, pp. 212–232, 1988.

[34] C. Edwards and S. Spurgeon, "Sliding mode control: Theory and applications." *Taylor and Francis.*, 1998.

[35] V. I. Utkin, "Sliding modes in control optimization, communication and control engineering series." *Springer-Verlag.*, 1992.

[36] W. Perruquetti and J. P. Barbot., "Sliding mode control in engineering." *Springer-Verlag, Berlin Heidelberg, 1 edition.*, 2009.

[37] B. Bandyopadhyay, F. Deepak, and K.-S. Kim, "Sliding mode control using novel sliding surfaces," vol. 392, 2009.

[38] İlyas Eker, "Sliding mode control with pid sliding surface and experimental application to an electromechanical plant," *ISA Transactions*, vol. 45, no. 1, pp. 109 – 118, 2006.

[39] M. Pachter and S. Banda, "Toward improvement on tracking performance — nonlinear feedback for linear systems," *International Journal of Control*, vol. 70, pp. 1–11, 1998.

[40] S. Mondal and C. Mahanta, "Nonlinear sliding surface based second order sliding mode controller for uncertain linear systems," *Communications in Nonlinear Science and Numerical Simulations*, vol. 16, no. 9, pp. 3760–3769, 2011.

[41] S. Newman, A. Nassehi, R. Imani-Asrai, and V. Dhokia, "Energy efficient process planning for cnc machining," *CIRP Journal of Manufacturing Science and Technology*, vol. 5, no. 2, pp. 127–136, 2012.

[42] J. B. Dahmus and T. G. Gutowski , "An Environmental Analysis of Machining," *In Proceedings of ASME International Mechanical Engineering Congress R and D Exposition*, pp. 13–19, 2004.

[43] A. Vijayaraghavan and D. Dornfeld, "Automated energy monitoring of machine tools," *CIRP Annals*, vol. 59, no. 1, pp. 21 – 24, 2010.

[44] A. Dietmair and A. Verl, "Energy consumption forecasting and optimisation for tool machines," *Modern Machinery Science Journal*, vol. 62, pp. 62–67, 2009.

[45] M. Zolgharni, B. Jones, R. Bulpett, A. Anson, and J. Franks, "Energy efficiency improvements in dry drilling with optimised diamond-like carbon coatings," *Diamond and Related Materials*, vol. 17, no. 7-10, pp. 1733–1737, 2008.

[46] L. Zhou, J. Li, F. Li, Q. Meng, J. Li, and X. Xu, "Energy consumption model and energy efficiency of machine tools: a comprehensive literature review," *Journal of Cleaner Production*, vol. 112, pp. 3721 – 3734, 2016.

[47] Y. He, Y. Li, T. Wu, and J. W. Sutherland, "An energy-responsive optimization method for machine tool selection and operation sequence in flexible machining job shops," *Journal of Cleaner Production*, vol. 87, pp. 245 – 254, 2015.

[48] H. S. Yoon, E. S. Kim, M. S. Kim, J. Y. Lee, G. B. Lee, and S. H. Ahn, "Towards greener machine tools – a review on energy saving strategies and technologies," *Renewable and Sustainable Energy Reviews*, vol. 48, pp. 870 – 891, 2015.

[49] S. Hu, F. Liu, Y. He, and T. Hu, "An on-line approach for energy efficiency monitoring of machine tools," *Journal of Cleaner Production*, vol. 27, no. Supplement C, pp. 133 – 140, 2012.

[50] U. Gotze, H. Koriath, A. Kolesnikov, R. Lindner, and J. Paetzold, "Integrated methodology for the evaluation of the energy and cost effectiveness of machine tools," *CIRP Journal of Manufacturing Science and Technology*, vol. 5, no. 3, pp. 151 – 163, 2012.

[51] O. I. Avram and P. Xirouchakis, "Evaluating the use phase energy requirements of a machine tool system," *Journal of Cleaner Production*, vol. 19, no. 6, pp. 699 – 711, 2011.

[52] R. Neugebauer, M. Wabner, H. Rentzsch, and S. Ihlenfeldt, "Structure principles of energy efficient machine tools," *CIRP Journal of Manufacturing Science and Technology*, vol. 4, no. 2, pp. 136 – 147, 2011.

[53] F. Draganescu, M. Gheorghe, and C. Doicin, "Models of machine tool efficiency and specific consumed energy," *Journal of Materials Processing Technology*, vol. 141, no. 1, pp. 9 – 15, 2003.

[54] C. Okwudire and J. Rodgers, "Design and control of a novel hybrid feed drive for high performance and energy efficient machining," *CIRP Annals*, vol. 62, no. 1, pp. 391 – 394, 2013.

[55] A. E. K. Mohammad, N. Uchiyama, and S. Sano, "Energy saving in feed drive systems using sliding-mode-based contouring control with a nonlinear sliding surface," *IEEE/ASME Transactions on Mechatronics*, vol. 20, no. 2, pp. 572–579, 2015.

[56] N. Uchiyama, Y. Ogawa, A. E. K. Mohammad, and S. Sano, "Energy saving in five-axis machine tools using synchronous and contouring control and verification by machining experiment," *IEEE Transactions on Industrial Electronics*, vol. 62, no. 9, pp. 5608–5618, 2015.

[57] N. Uchiyama, K. Goto, and S. Sano, "Analysis of energy consumption in fundamental motion of industrial machines and experimental verification," in *2015 American Control Conference (ACC)*, 2015, pp. 2179–2184.

[58] B. Bandyopadhyay and D. Fulwani, "High-performance tracking controller for discrete plant using nonlinear sliding surface," *IEEE Transactions on Industrial Electronics*, vol. 56, no. 9, pp. 3628–3637, 2009.

[59] Z. Lin, M. Pachter, and S. Banda, "Toward improvement of tracking performance nonlinear feedback for linear systems," *International Journal of Control*, vol. 70, no. 1, pp. 1–11, 1998.

[60] Y. He, B. M. Chen, and C. Wu, "Improving transient performance in tracking control for linear multivariable discrete-time systems with input saturation," *Systems & Control Letters*, vol. 56, no. 1, pp. 25 – 33, 2007.

[61] G. Cheng, K. Peng, B. M. Chen, and T. H. Lee, "Improving transient performance in tracking general references using composite nonlinear feedback control and its application to high-speed xy-table positioning mechanism," *IEEE Transactions on Industrial Electronics*, vol. 54, no. 2, pp. 1039–1051, 2007.

[62] B. Bandyopadhyay and D. Fulwani, "A robust tracking controller for uncertain mimo plant using non-linear sliding surface," in *IEEE International Conference on Industrial Technology*, 2009, pp. 1–6.

[63] M. Chen, S. S. Ge, and B. Ren, "Adaptive tracking control of uncertain mimo nonlinear systems with input constraints," *Automatica*, vol. 47, no. 3, pp. 452 – 465, 2011.

[64] H. Zhang and F. L. Lewis, "Adaptive cooperative tracking control of higher-order nonlinear systems with unknown dynamics," *Automatica*, vol. 48, no. 7, pp. 1432 – 1439, 2012.

[65] H. Du, S. Li, and C. Qian, "Finite-time attitude tracking control of spacecraft with application to attitude synchronization," *IEEE Transactions on Automatic Control*, vol. 56, no. 11, pp. 2711–2717, 2011.

[66] Z. Li, X. Liu, W. Ren, and L. Xie, "Distributed tracking control for linear multiagent systems with a leader of bounded unknown input," *IEEE Transactions on Automatic Control*, vol. 58, no. 2, pp. 518–523, 2013.

[67] P. Ouyang, J. Acob, and V. Pano, "PD with sliding mode control for trajectory tracking of robotic system," *Robotics and Computer-Integrated Manufacturing*, vol. 30, no. 2, pp. 189 – 200, 2014.

[68] B. Sencer, K. Ishizaki, and E. Shamoto, "A curvature optimal sharp corner smoothing algorithm for high-speed feed motion generation of nc systems along linear tool paths," *The International Journal of Advanced Manufacturing Technology*, vol. 76, no. 9, pp. 1977–1992, 2015.

[69] "Bezier curve based trajectory generation and nonlinear friction compensation for feed drive contouring control," *IFAC Papers On Line*, vol. 50, no. 1, pp. 1944 – 1951, 2017.

[70] J. Zheng, H. Wang, Z. Man, J. Jin, and M. Fu, "Robust motion control of a linear motor positioner using fast nonsingular terminal sliding mode," *IEEE/ASME Transactions on Mechatronics*, vol. 20, no. 4, pp. 1743–1752, 2015.

[71] X. Li, H. Zhao, X. Zhao, and H. Ding, "Dual sliding mode contouring control with high accuracy contour error estimation for five-axis cnc machine tools," *International Journal of Machine Tools and Manufacture*, vol. 108, pp. 74 – 82, 2016.

[72] X. C. Xi, W. S. Zhao, and A. N. Poo, "Improving cnc contouring accuracy by robust digital integral sliding mode control," *International Journal of Machine Tools and Manufacture*, vol. 88, pp. 51 – 61, 2015.

[73] J. Yang and Y. Altintas, "A generalized on-line estimation and control of five-axis contouring errors of cnc machine tools," *International Journal of Machine Tools and Manufacture*, vol. 88, pp. 9 – 23, 2015.

[74] L. Dong and W. C. Tang, "Adaptive backstepping sliding mode control of flexible ball screw drives with time-varying parametric uncertainties and disturbances," *ISA Transactions*, vol. 53, no. 1, pp. 110 – 116, 2014.

[75] M. R. Msukwa, N. Uchiyama, and B. D. Bui, "Adaptive nonlinear sliding mode control with a nonlinear sliding surface for feed drive systems," in *2017 IEEE International Conference on Industrial Technology (ICIT)*, 2017, pp. 732–737.

[76] A. E. K. Mohammad, N. Uchiyama, and S. Sano, "Reduction of electrical energy consumed by feed-drive systems using sliding-mode control with a nonlinear sliding surface," *IEEE Transactions on Industrial Electronics*, vol. 61, no. 6, pp. 2875–2882, 2014.

[77] J. J. Slotine and S. S. Sastry, "Tracking control of non-linear systems using sliding surfaces, with application to robot manipulators," *International Journal of Control*, vol. 38, no. 2, pp. 465–492, 1983.

[78] R. Ortega and Y. Tang, "Robustness of adaptive controllers—a survey," *Automatica*, vol. 25, no. 5, pp. 651 – 677, 1989.

[79] G. Bartolini, A. Ferrara, and V. Utkin, "Adaptive sliding mode control in discrete-time systems," *Automatica*, vol. 31, no. 5, pp. 769 – 773, 1995.

[80] Shaocheng Tong and Han-Xiong Li, "Fuzzy adaptive sliding-mode control for mimo nonlinear systems," *IEEE Transactions on Fuzzy Systems*, vol. 11, no. 3, pp. 354–360, 2003.

[81] J. Lee and V. Utkin, "Chattering suppression methods in sliding mode control systems," *Annual Reviews in Control*, vol. 31, pp. 179–188, 2007.

[82] Y. Huang, T. Kuo, and S. Chang, "Adaptive sliding-mode control for nonlinearsystems with uncertain parameters," *IEEE Transactions on Systems, Man, and Cybernetics, Part B (Cybernetics)*, vol. 38, no. 2, pp. 534–539, 2008.

[83] L. B. Li, L. L. Sun, S. Z. Zhang, and Q. Q. Yang, "Speed tracking and synchronization of multiple motors using ring coupling control and adaptive sliding mode control," *ISA Transactions*, vol. 58, pp. 635 – 649, 2015.

[84] H. Li, P. Shi, D. Yao, and L. Wu, "Observer-based adaptive sliding mode control for nonlinear markovian jump systems," *Automatica*, vol. 64, pp. 133 – 142, 2016.

[85] A. Farrage and N. Uchiyama, "Adaptive sliding mode contouring control with a nonlinear sliding surface for feed drive systems," in *2017 56th Annual Conference of the Society of Instrument and Control Engineers of Japan (SICE)*, 2017, pp. 230–235.

[86] A. Merabet, R. Beguenane, J. S. Thongam, and I. Hussein, "Adaptive sliding mode speed control for wind turbine systems," in *IECON 2011 - 37th Annual Conference of the IEEE Industrial Electronics Society*, 2011, pp. 2461–2466.

[87] F. Plestan, Y. Shtessel, V. Bregeault, and A. Poznyak, "New methodologies for adaptive sliding mode control," *International Journal of Control*, vol. 83, no. 9, pp. 1907–1919, 2010.

[88] X. Xu, G. Y. Gu, Z. Xiong, X. Sheng, and X. Zhu, "Development of a decentralized multi-axis synchronous control approach for real-time networks," *ISA Transactions*, vol. 68, pp. 116 – 126, 2017.

[89] B. Zhu and R. T. Farouki, "A general framework for solving inverse dynamics problems in multi-axis motion control," *ISA Transactions*, vol. 95, pp. 130 – 143, 2019.

[90] K. R. Simba, B. D. Bui, M. R. Msukwa, and N. Uchiyama, "Robust iterative learning contouring controller with disturbance observer for machine tool feed drives," *ISA Transactions*, vol. 75, pp. 207 – 215, 2018.

[91] C. H. Wu and Y. T. Kung, "Thermal analysis for the feed drive system of a cnc machine center," *International Journal of Machine Tools and Manufacture*, vol. 43, no. 15, pp. 1521 – 1528, 2003.

[92] Y. Altintas, A. Verl, C. Brecher, L. Uriarte, and G. Pritschow, "Machine tool feed drives," *CIRP Annals*, vol. 60, no. 2, pp. 779 – 796, 2011.

[93] J. U. Cho, Q. N. Le, and J. W. Jeon, "An fpga-based multiple-axis motion control chip," *IEEE Transactions on Industrial Electronics*, vol. 56, no. 3, pp. 856–870, 2009.

[94] P. Li and G. Zhu, "Robust internal model control of servo motor based on sliding mode control approach," *ISA Transactions*, vol. 93, pp. 199 – 208, 2019.

[95] Y. Xie, X. Tang, B. Song, X. Zhou, and Y. Guo, "Data-driven adaptive fractional order pi control for pmsm servo system with measurement noise and data dropouts," *ISA Transactions*, vol. 75, pp. 172 – 188, 2018.

[96] W. Zhang, N. Nan, Y. Yang, W. Zhong, and Y. Chen, "Force ripple compensation in a pmlsm position servo system using periodic adaptive learning control," *ISA Transactions*, vol. 95, pp. 266–277, 2019.

[97] J. Yao, G. Yang, Z. Jiao, and D. Ma, "Adaptive robust motion control of direct-drive dc motors with continuous friction compensation," *Hindawi Publishing Corporation*, vol. 2013, 2013.

[98] W. Deng and J. Yao, "Adaptive integral robust control and application to electromechanical servo systems," *ISA Transactions*, vol. 67, pp. 256 – 265, 2017.

[99] S. Wang, J. Na, H. Yu, and Q. Chen, "Finite time parameter estimation-based adaptive predefined performance control for servo mechanisms," *ISA Transactions*, vol. 87, pp. 174 – 186, 2019.

[100] S. Y. Chen, T. H. Li, and C. H. Chang, "Intelligent fractional-order backstepping control for an ironless linear synchronous motor with uncertain nonlinear dynamics," *ISA Transactions*, vol. 89, pp. 218 – 232, 2019.

[101] J. Yao, Z. Jiao, and D. Ma, "Rise-based precision motion control of dc motors with continuous friction compensation," *IEEE Transactions on Industrial Electronics*, vol. 61, no. 12, pp. 7067–7075, 2014.

[102] C. Li, C. Li, Z. Chen, and B. Yao, "Advanced synchronization control of a dual-linear-motor-driven gantry with rotational dynamics," *IEEE Transactions on Industrial Electronics*, vol. 65, no. 9, pp. 7526–7535, 2018.

[103] Z. Chen, C. Li, B. Yao, M. Yuan, and C. Yang, "Integrated coordinated/synchronized contouring control of a dual-linear-motor-driven gantry," *IEEE Transactions on Industrial Electronics*, vol. 67, no. 5, pp. 3944–3954, 2019.

[104] R. Raman, A. Chalanga, S. Kamal, and B. Bandyopadhyay, "Nonlinear sliding surface based adaptive sliding mode control for industrial emulator," *2013 IEEE International Conference on Industrial Technology (ICIT)*, pp. 124–129, 2013.

[105] M. R. Msukwa, N. Uchiyama, and B. D. Bui, "Adaptive nonlinear sliding mode control with a nonlinear sliding surface for feed drive systems," *Industrial Technology (ICIT), 2017 IEEE International Conference on*, pp. 732–737, 2017.

[106] M. R. Msukwa and N. Uchiyama, "Design and experimental verification of adaptive sliding mode control for precision motion and energy saving in feed drive systems," *IEEE Access*, vol. 7, pp. 20 178–20 186, 2019.

[107] A. Elfizy, G. Bone, and M. Elbestawi, "Model-based controller design for machine tool direct feed drives," *International Journal of Machine Tools and Manufacture*, vol. 44, no. 5, pp. 465 – 477, 2004.

[108] A. Kamalzadeh, D. J. Gordon, and K. Erkorkmaz, "Robust compensation of elastic deformations in ball screw drives," *International Journal of Machine Tools and Manufacture*, vol. 50, no. 6, pp. 559 – 574, 2010.

[109] J. Yao, W. Deng, and Z. Jiao, "Adaptive control of hydraulic actuators with lugre model-based friction compensation," *IEEE Transactions on Industrial Electronics*, vol. 62, no. 10, pp. 6469–6477, 2015.

[110] A. Verl and S. Frey, "Correlation between feed velocity and preloading in ball screw drives," *CIRP Annals*, vol. 59, no. 1, pp. 429 – 432, 2010.

[111] S. Yamada, H. Fujimoto, and Y. Terada, "Joint torque control for backlash compensation in two-inertia system," in *2016 IEEE 25th International Symposium on Industrial Electronics (ISIE)*, 2016, pp. 1138–1143.

[112] E. Kayacan and J. Peschel, "Robust model predictive control of systems by modeling mismatched uncertainty," *IFAC Papers On Line*, vol. 49, no. 18, pp. 265–269, 2016.

[113] D. Prévost, S. Lavernhe, C. Lartigue, and D. Dumur, "Feed drive modelling for the simulation of tool path tracking in multi-axis high speed machining," *International Journal of Mechatronics and Manufacturing Systems*, vol. 4, no. 3-4, pp. 266–284, 2011.

[114] Y. Su, D. Sun, and B. Duan, "Design of an enhanced nonlinear pid controller," *Mechatronics*, vol. 15, no. 8, pp. 1005–1024, 2005.

[115] M. Weck and G. Ye, "Sharp corner tracking using the ikf control strategy," *CIRP Annals*, vol. 39, no. 1, pp. 437 – 441, 1990.

[116] M. R. Msukwa, E. W. Nshama, and N. Uchiyama, "Adaptive sliding mode control for precision motion of industrial feed drive systems with uncertainty dynamics," in *2019 American Control Conference (ACC)*, 2019, pp. 1718–1723.

[117] C. Hu, B. Yao, and Q. Wang, "Coordinated adaptive robust contouring controller design for an industrial biaxial precision gantry," *Mechatronics, IEEE/ASME Transactions on*, vol. 15, pp. 728 – 735, 2010.

[118] Y. Koren, "Cross-coupled biaxial computer control for manufacturing systems," *Journal of Dynamic Systems Measurement and Control*, vol. 102, pp. 265 – 271, 1980.

[119] S. Yeh and P. Hsu, "Estimation of the contouring error vector for the cross-coupled control design," *IEEE/ASME Transactions on Mechatronics*, vol. 7, pp. 44–51, 2002.

[120] S. L. Chen, H. Liu, and S. Ting, "Contouring control of biaxial systems based on polar coordinates," *Mechatronics, IEEE/ASME Transactions on*, vol. 7, pp. 329 – 345, 2002.

[121] N. Uchiyama, T. Nakamura, and H. Yanagiuchi, "The effectiveness of contouring control and a design for three-dimensional machining," *International Journal of Machine Tools and Manufacture*, vol. 49, no. 11, pp. 876 – 884, 2009.